

# Performance investigation of a loop heat pipe integrated with thermoelectric cooler under acceleration field

Zhen Fang<sup>a</sup>, Yongqi Xie<sup>a</sup>, Yanmeng Xu<sup>b</sup>, Hongwei Wu<sup>c,\*</sup>, Hongxing Zhang<sup>d,\*\*</sup>, Longzhu Han<sup>e</sup>

<sup>a</sup>School of Aeronautic Science and Engineering, Beihang University, Beijing, 100191, China

<sup>b</sup>Cleaner Electronics Group, College of Engineering, Design and Physical Sciences, Brunel University, London, Uxbridge, UK

<sup>c</sup>School of Physics, Engineering and Computer Science, University of Hertfordshire, Hatfield, AL10 9AB, UK

<sup>d</sup>Beijing Key Laboratory of Space Thermal Control Technology, China Academy of Space Technology, Beijing 100094, China

<sup>e</sup>School of Biological Science and Medical Engineering, Beihang University, Beijing, 100191, China

\*Corresponding Author (Dr. Hongwei Wu): Email: h.wu6@herts.ac.uk

\*\*Corresponding Author (Dr. Hongxing Zhang): Email: redstarbenben@163.com

## ABSTRACT

This paper presents an experimental investigation on a novel dual compensation chamber loop heat pipe (DCCLHP) integrated with thermoelectric cooler (TEC) for improving the overall performance under various acceleration conditions. The operating characteristics of the DCCLHP with and without the assistance of TEC for configurations A and B are analyzed systematically under different acceleration magnitudes and heat loads. The heat load on the evaporator ranged from 25 W to 300 W. The power of the TEC was 10 W. The acceleration magnitude ranged from 5 g to 13 g. Experimental results show that: (i) the application of TEC is proved to improve the operating performance at the heat load not exceeding 150 W under configuration A and 100 W under configuration B; (ii) under configuration B, the increase of the acceleration normally leads to the increase of the operating temperature and the decrease of the thermal conductance. While it shows no obvious effect on the operating performance under configuration A for most cases. The maximum operating temperature and thermal conductance is 56.7 °C at 150 W under 13 g for configuration B, while 20.7 W/K at 150 W under 5 g for configuration A; (iii) temperature fluctuation occurs at 100 W under 5 g and 7 g for configuration B, whereas there is no fluctuation under configuration A. The acceleration effect can change the vapor-liquid distribution in the loop and the external loop pressure drop, and further change the operating performance along with the TEC effect. This research provides valuable insight into the influence of TEC on DCCLHP under the acceleration field, which is of great significance for its practical application in mechanical and aerospace engineering.

**KEY WORDS:** Loop heat pipe, dual compensation chamber, acceleration field, thermoelectric cooler, operating characteristics

## 1. INTRODUCTION

Loop heat pipe (LHP) is a high efficient and reliable two-phase heat transfer device, which utilizes the vapor-liquid phase change of working liquid in evaporator and condenser [1-3]. Compared with traditional heat pipe, LHP possess the advantages of long-distance heat transfer capability, flexible installation, precise temperature control and anti-overload acceleration [4-6]. Over the past three decades, LHPs have been widely applied in various aircraft, spacecraft and electronic cooling equipment [7-11]. Different from conventional LHP, the dual compensation chamber loop heat pipe (DCCLHP) has two compensation chambers (CCs) distributed at both ends of the evaporator, which enables the capillary core to be more effectively infiltrated under gravity field or acceleration field [12-13]. Some previous researches have proven that DCCLHP could work successfully under some extreme conditions such as anti-gravity or subjected to acceleration forces [14-15].

Many researchers have conducted both experimental and theoretical studies on the operating characteristics of DCCLHP. Gerhart and Gluck tested the performance of a set of ammonia working fluid in DCCLHP, which proved its ability to operate under different evaporator and CC orientations [16]. It was found that the condenser temperature changes could lead to temperature fluctuations and reverse flow during start-up when the heat load is less than 50 W. Afterwards, they conducted a further study on the operating characteristics of DCCLHP with nine different configurations under gravity field [17-18]. Long et al. [19] experimentally studied the performance of DCCLHP under different heat loads, frequencies, waveforms and operating attitudes. It was revealed that the start-up temperature rise and operating temperature increased with the increase of evaporator tilt angle. The operating performance under cyclical heat load with a frequency greater than 0.1 Hz was similar to that of constant heat load. Zhang et al. [12] conducted experimental tests on a set of DCCLHP developed by the China Academy of Space Technology. Their experimental results showed that DCCLHP could operate and start-up normally in any direction of gravity, but the operation and the thermal control characteristics of the DCCLHP were different from that for the conventional LHP. They also introduced a new design method of the working fluid charge mass and the CC volumes, which could effectively avoid the most difficult situation for DCCLHP to start-up. Their results had shown the potential application of loop heat pipes in aircraft thermal management systems. A systematic investigation of the start-up and steady-state performance of DCCLHPs at different relative orientations between the evaporator and CCs under gravitational surroundings was conducted by Bai et al. [20]. It was stated that it could start normally at 5 W, but sometimes the start temperature rise was higher. They also presented that the difference in the vapor-liquid distribution in the evaporator and the heat leakage from the evaporator to the CC could be the reasons for different start-up performance under the same heat load and different layout positions.

Visualization is an important method to explore the flow mechanism inside the loop. Lin et al. [21] designed an experiment to observe the flow of ammonia inside the two CCs and condenser of DCCLHP. Their research revealed several interesting phenomena inside the loop, such as bubble generation in the evaporator liquid core, reverse flow, fluctuated flow and liquid re-distribution. They concluded that the unique operating performance of DCCLHP was attributed to the change in vapor-liquid distribution and the radial heat leakage of the evaporator. Zhao et al. [22] experimentally studied the operation of the stainless steel-ethanol DCCLHP anti-icing system under different heat loads and angles of attack. By visualizing the CCs, they observed that changes in the relative positions of CC1 and CC2 will change the distribution of working fluids in the two CCs. They also found that the angle of attack could seriously affect the operating temperature of DCCLHP, and could even lead to temperature oscillations in the entire loop. Bai et al. [23] designed a new DCCLHP structure, which extends the length of the liquid guide tube to improve the performance of DCCLHP especially at small heat load. They demonstrated that the extended bayonet tube could increase the cooling of CC2, thereby improving the start-up performance of DCCLHP.

It is recognized that the performance of DCCLHP can change when it is subjected to acceleration forces. Xie et al. [24-25] could be the first to systematically study the performance of DCCLHP under acceleration fields. In the research work of [24], a combined experimental research and theoretical analysis were conducted on the performance of DCCLHP under both gravitational field and acceleration field. They proposed a novel acceleration force assist concept for the phenomena observed in their experiments. It was found that DCCLHP can be operated in centrifugal force drive or capillary force-centrifugal force co-drive mode. When the heat load is less than 100 W, the effect of acceleration on the operating temperature is very significant. The operating temperature under accelerated conditions is significantly lower than the operating temperature under terrestrial gravity. Ref. [25] conducted an experimental study on the transient performance of DCCLHP under periodic acceleration field. Their results showed that the loop temperature will periodically oscillate with the periodic changes of acceleration, and larger acceleration may lead to higher operating temperature.

During each periodic acceleration, loop temperature oscillations with different frequencies and amplitudes may also occur.

It has been noted that several researchers have attempted to use TEC to control the operating temperature of LHP. Ku et al. [26-28] conducted a comprehensive theoretical and experimental research on using TECs for operating temperature control of a LHP. In their research, bipolar power supply and control algorithms were used to allow TEC to heat or cool CC according to the set temperature. Their ground experiments had proved that TEC could effectively control the temperature of CC within 0.3 K of the set point. In addition, the experiments conducted by Ku et al. showed that the power required to use TEC to control the temperature of LHP was much smaller compared with traditional electric heaters. Franzoso et al. [29] designed a set of TEC-LHP equipment and conducted a thermal vacuum test. They concluded that TEC could make full use of the condenser by balancing the heat leakage from evaporator to CC. However, they found that both gravity and heat leakage to the environment would greatly limit the effect of TEC on LHP temperature under large heat loads, and even larger TEC power would have a negative effect on the loop. In their study, TEC showed its ability to suppress the natural oscillations of the LHP. Yang et al. [30] experimentally studied the effect of TEC on this LHP, which was filled with a small amount of nitrogen as a non-condensable gas (NCG). Their research showed that TEC could reduce the steady-state operating temperature of LHP with NCG, and greatly reduced the temperature overshoot during start-up. In addition, they found that TEC could eliminate or suppress possible temperature fluctuations. Xie et al. [31] conducted an experimental study to investigate the effect of TEC on DCCLHP under different heat loads and accelerations. They found that in some cases, TEC assistance could improve the performance of DCCLHP start-up and reduce the operating temperature. However, their study limited to the cases where the acceleration was parallel to the evaporator and was not conducive to the direction of the liquid working fluid backflow.

It appears from the previous investigations that both TEC and acceleration could have a significant impact on the performance of DCCLHP. However, there are few researchers have studied the effect of TEC assisting the start-up and operation of DCCLHP under various acceleration conditions. To the best of the authors' knowledge, there are no research works focus on the effects of TEC on the performance of DCCLHP under different acceleration magnitudes and directions. In order to improve the performance of DCCLHP on aircraft, it is imperative to explore the effect of TEC on DCCLHP under high acceleration fields in a systematic manner.

## 2. EXPERIMENTAL SETUP

### 2.1. Experimental apparatus

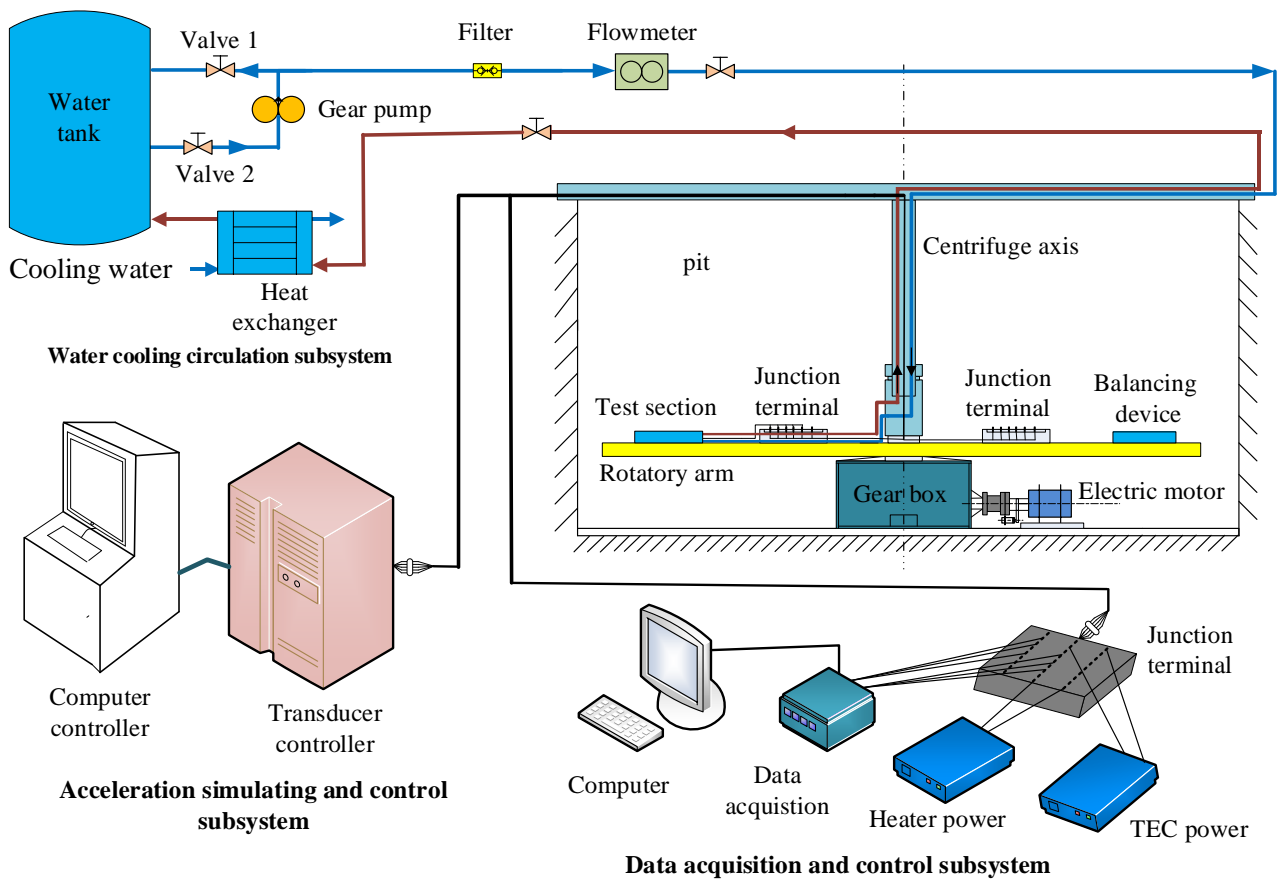
Fig. 1 (a) and (b) shows the schematic diagram and photograph of the experimental setup used in the current work, respectively. The experimental apparatus mainly includes a test section, an acceleration simulation and control system, a cooling water circulation system, and a signal measurement system. The test section is a stainless steel-ammonia DCCLHP, which consists of evaporator, condenser, CC, vapor line and liquid line. CCs were designed at both ends of the evaporator to ensure that the evaporator can also be supplied with liquid even for extreme cases. The internal structure of evaporator and CC is demonstrated in Fig. 2 and the specific parameters are listed in Table 1.

As presented in Fig. 3(a), the TEC is fixed to CC by a saddle-shaped mounting seat. The cold side of the TEC is close to the CC, while the hot side is close to the thermally conductive copper block. The heat can be transferred from the hot side of the TEC to the evaporator through the thermal bridge that is made of copper block with good thermal conductance. During the experiment, the power of each TEC is set to 10 W, and both TECs are turned on and off simultaneously. The heat load is applied to the evaporator through a kapton heater that tightly attached to the outer surface of the evaporator, as

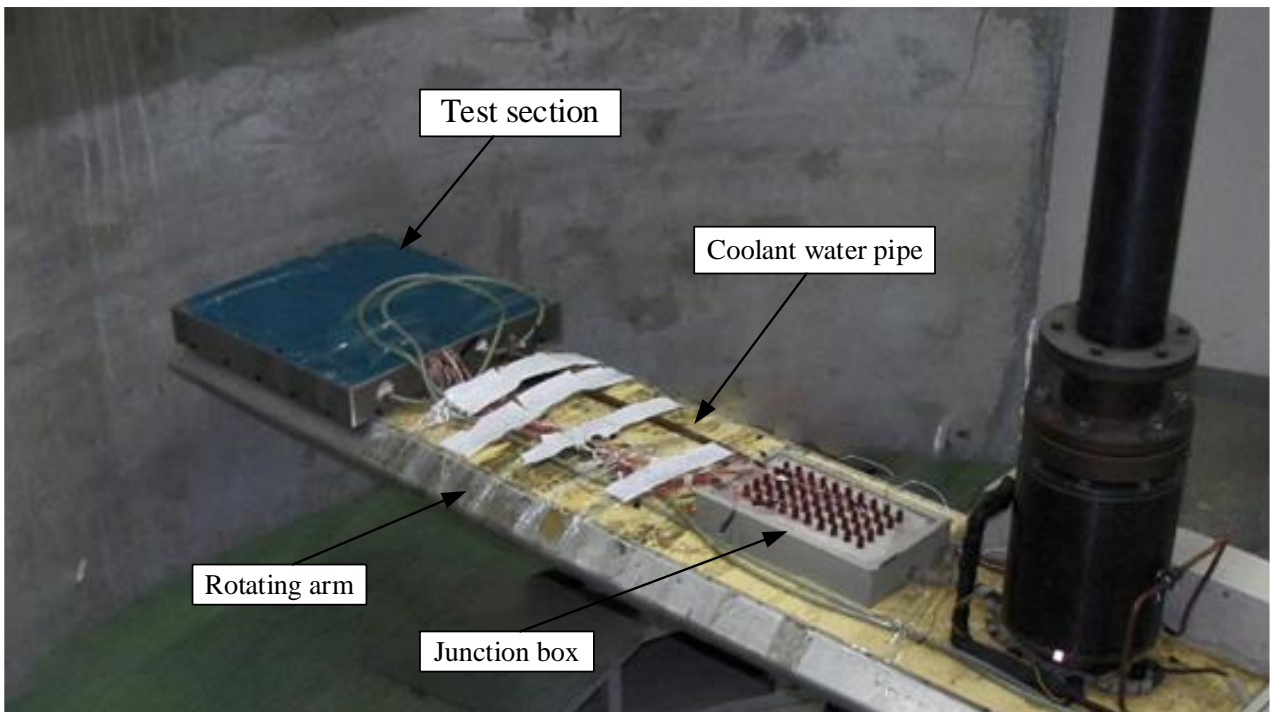
shown in Fig. 3(b). Different heat loads can be achieved by adjusting the output current of the DC power supply. In the current work, the kapton heater is well insulated, therefore it can be assumed that all the heat load is applied to the evaporator.

The acceleration simulation and control system is composed of rotating arm, gear box, electric motor and acceleration control section. A counterweight with the same mass is installed on the other end in order to balance the arm. The electric motor drives the arm of the centrifuge to rotate. At the low speed mode, the maximum acceleration of 13 g can be generated at the test section. The acceleration controller can control the speed of the centrifuge with an accuracy of  $\pm 5\%$ . Taking the safety issue into consideration, in the current work, the maximum rotation time of the turntable is not more than one hour.

The signal measurement system is mainly composed of temperature sensor, data acquisition board, Agilent data acquisition instrument and a computer. The temperature sensor uses Pt100 with an accuracy of  $\pm 0.3$  °C. In order to eliminate the measurement error, all Pt100 wiring uses a four-wire connection method. The electric slip rings are installed inside the centrifuge axis to ensure that the signal can be successfully collected during the centrifugal operation.



(a) Schematic diagram of the experimental system



(b) Photograph of experimental setup

**Fig. 1.** Schematic diagram and photograph of experimental system.

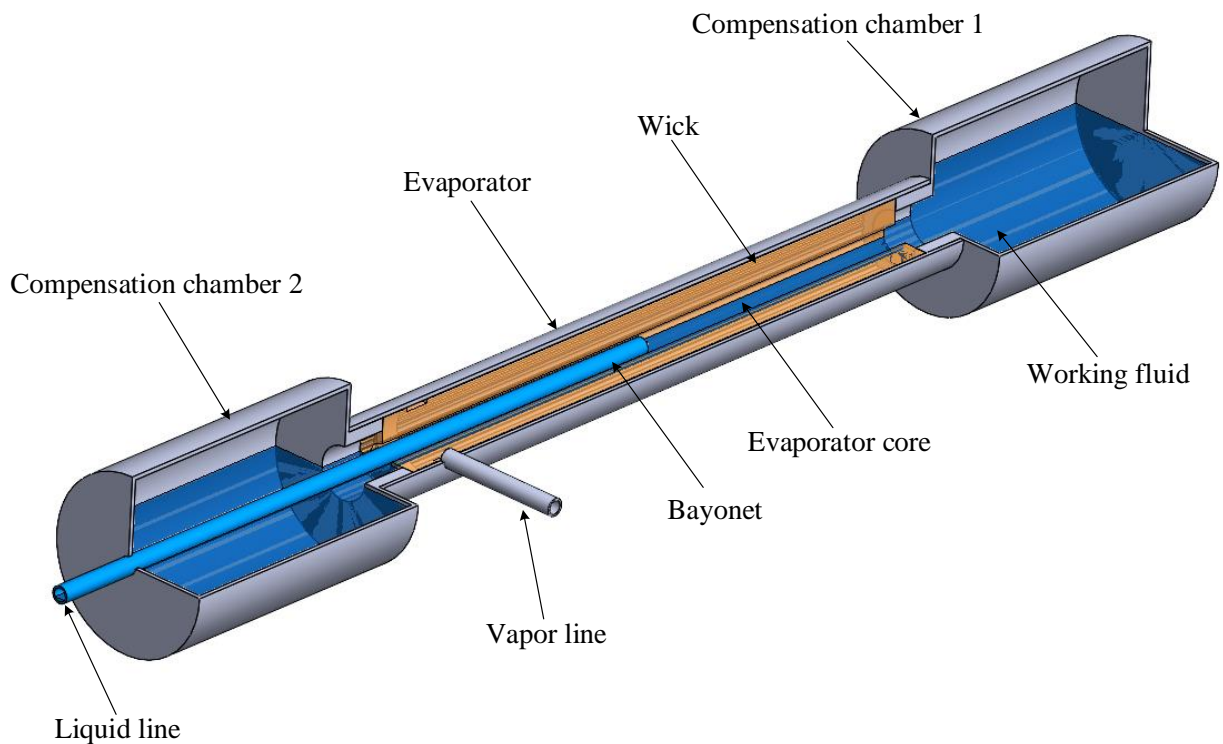


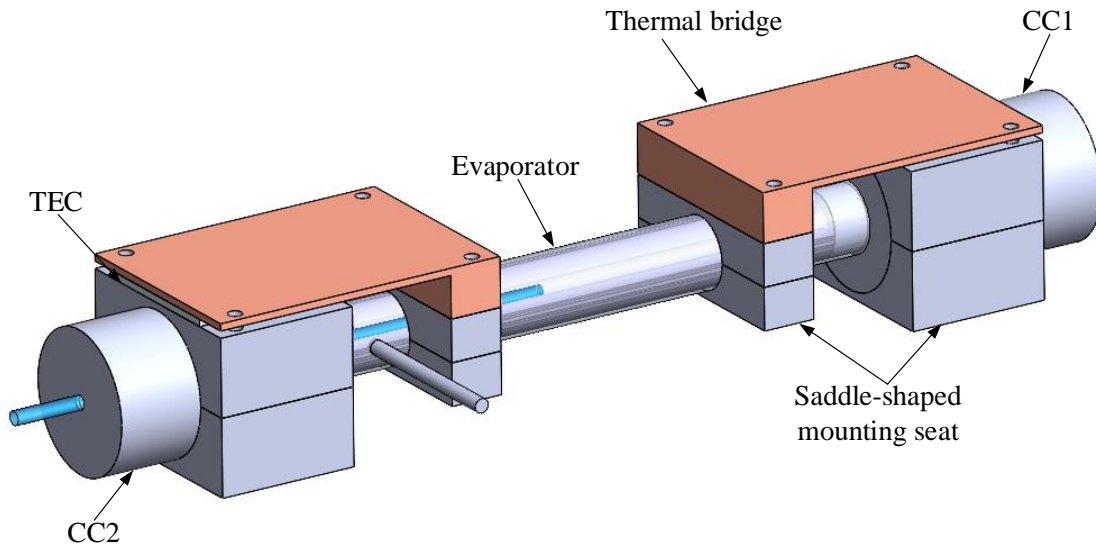
**Fig. 2.** Internal Structure of Evaporator and CC.

The cooling water circulation system mainly includes the thermostatic water tank, gear pump, mass flow meter, plate heat exchanger and cold plate. The gear pump drives the cooling water from the thermostatic water tank to the DCCLHP condensate plate. The cooling water is heated in the cold

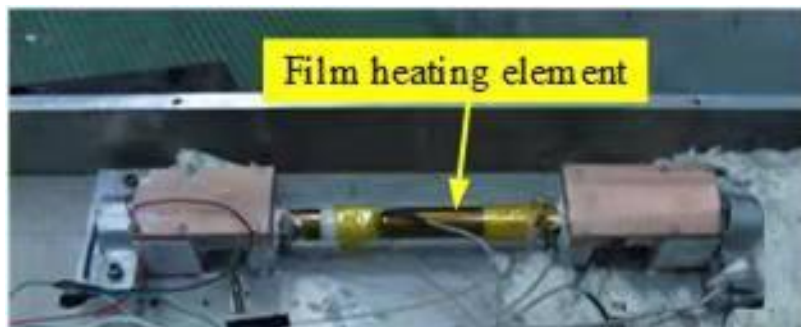
plate and then returns to the thermostatic water tank for recirculation. Liquid collecting rings was installed in the centrifuge axis to ensure that the cooling water can reach the test section when the centrifuge is rotating. Plate heat exchanger was designed to prevent the temperature of the backflow cooling water from being too high, and the heat brought back exceeds the load of the thermostatic water tank. The cooling water mass flow can be accurately measured by mass flow meter (DMF-1-2) with an accuracy of  $\pm 0.05\%$ . Throughout the experiment, the temperature of the circulating cooling water was controlled at 21 °C.

**Table 1** Components, material and geometric parameters of DCCLHP

Components	Parameter	Dimensions
Evaporator (Stainless steel)	OD/ID×Length/mm	20/18×209
Wick (Nickel)	OD/ID×Length/mm	18/6×190
	Porosity	55%
	Permeability/m <sup>2</sup>	$\geq 5 \times 10^{-14}$
	Pore radius/ $\mu\text{m}$	1.5
Compensation chamber (Stainless steel)	OD/ID×Length/mm	27/25×64
	Number	2
Vapor line (Stainless steel)	OD/ID×Length/mm	3/2.6×1100
Condenser line (Stainless steel)	OD/ID×Length/mm	3/2.6×2530
Liquid line (Stainless steel)	OD/ID×Length/mm	3/2.6×400



(a) TEC installation

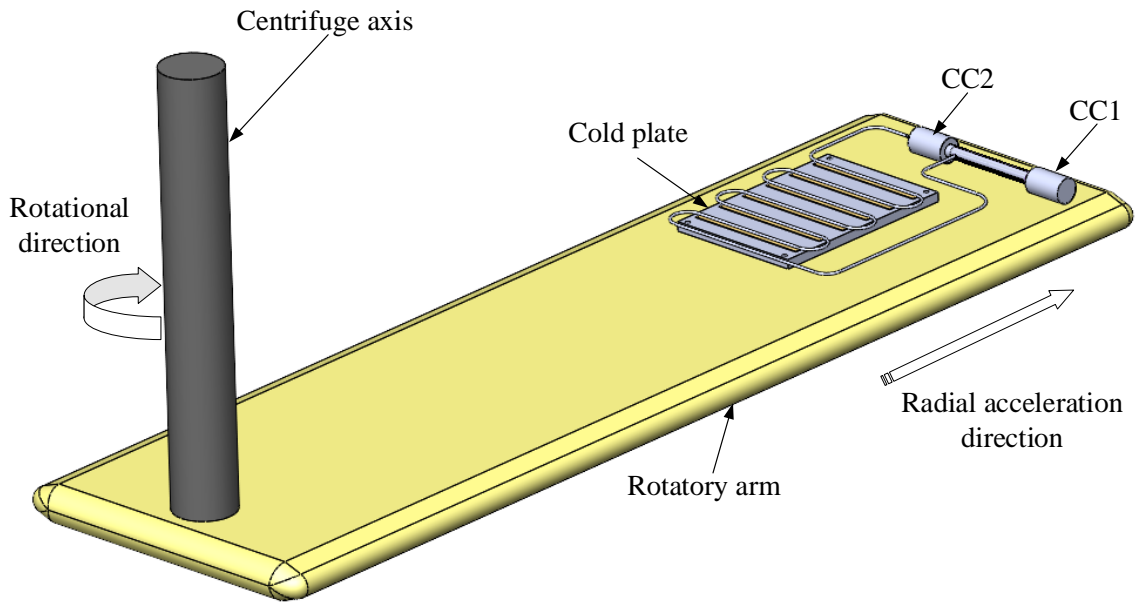


(b) Heater attached to the evaporator

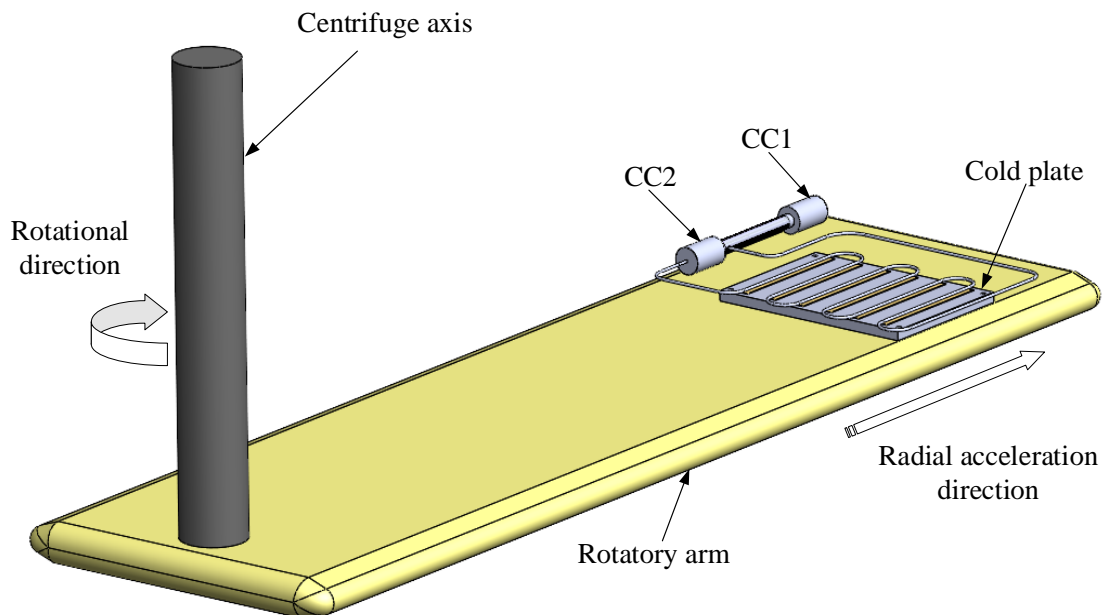
**Fig. 3.** Diagram of TEC installation and photograph of heater attached to the evaporator.

## 2.2. Experimental conditions

In the current work, DCCLHP is installed horizontally along the rotating arm with two different directions, as shown in Fig. 4. In Fig. 4(a), the acceleration direction is perpendicular to the evaporator and points to the evaporator from the condenser, which is referred to as configuration A. In Fig. 4(b), configuration B is defined as the acceleration direction is parallel to the evaporator and points to the CC1 from the CC2. In order to fully explore the operational performance of DCCLHP under different acceleration field, experiments are carried out with a wide range of heat loads (25 W, 100 W, 150 W, 200 W, 250 W, 300 W) with five different acceleration magnitudes (5 g, 7 g, 9 g, 11 g, 13 g). For the purpose of comparison, all experiments are conducted with and without the assistance of TEC.



(a) Configuration A



(b) Configuration B

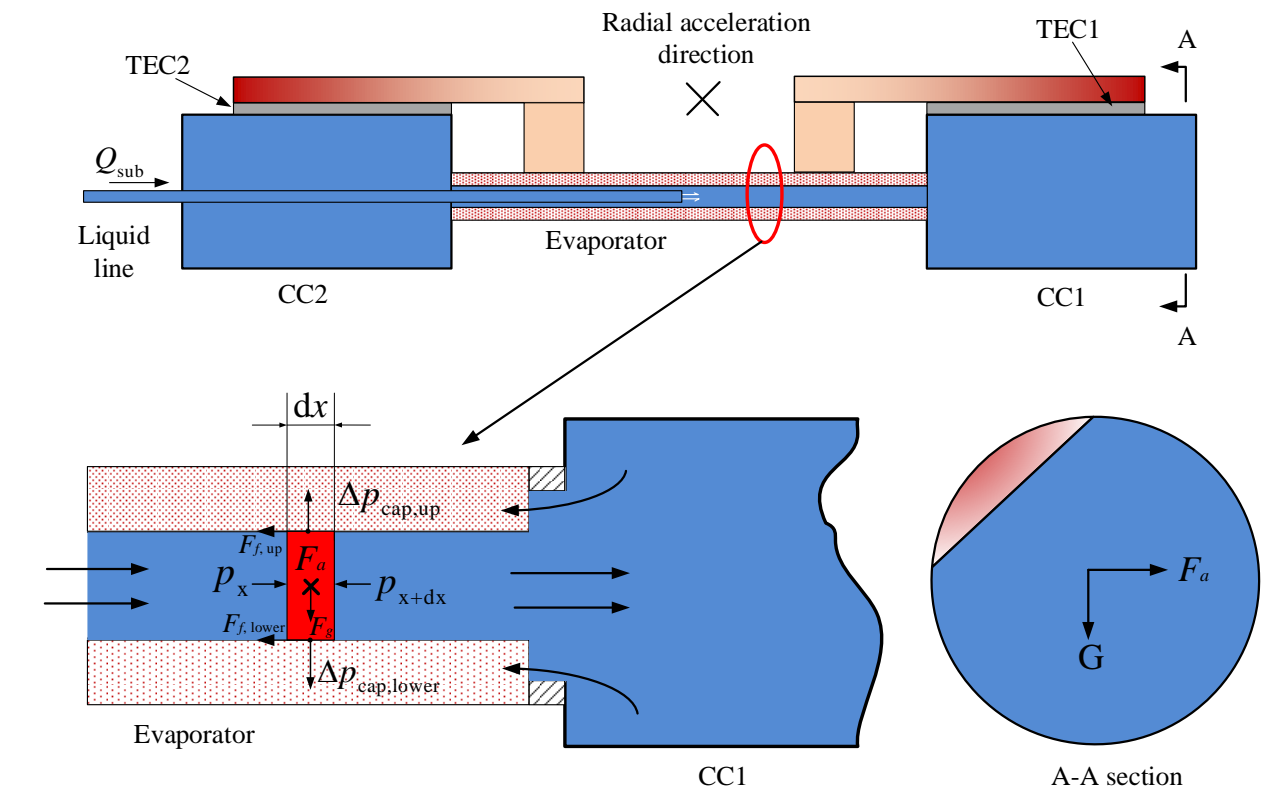
**Fig. 4.** Schematic diagram of acceleration direction.

In order to investigate the effect of gravitational/centrifugal force on the direction of the working fluid under above two configurations during the operation, it could be better to have a good understanding of the force balance of the system. Fig. 5 shows the force balance diagram of a microelement unit ( $dx$ ) of the working fluid in the evaporator core. The wick is a porous medium with a complicated internal structure, and the liquid in it is mainly driven by capillary force. Since the wick of the LHP can be infiltrated at both ends, it is of little significance to conduct force equilibrium analysis on the liquid. Therefore, the evaporator core that is filled with working fluid when LHP reaches a stable operation is selected for analysis. Under configuration A, it is mainly affected by several control parameters such as gravity, acceleration force, capillary force and differential pressure drag and friction drag. Since the direction of the liquid movement is perpendicular to the direction of angular velocity of rotation, thus, it will not be affected by the Coriolis force. Under configuration B, the microelement unit is also affected by the above forces in addition to the Coriolis force. From the above analysis, the acceleration force under configuration B is more conducive to promoting the flow of working fluid between the evaporator and CC1 than that under configuration A.

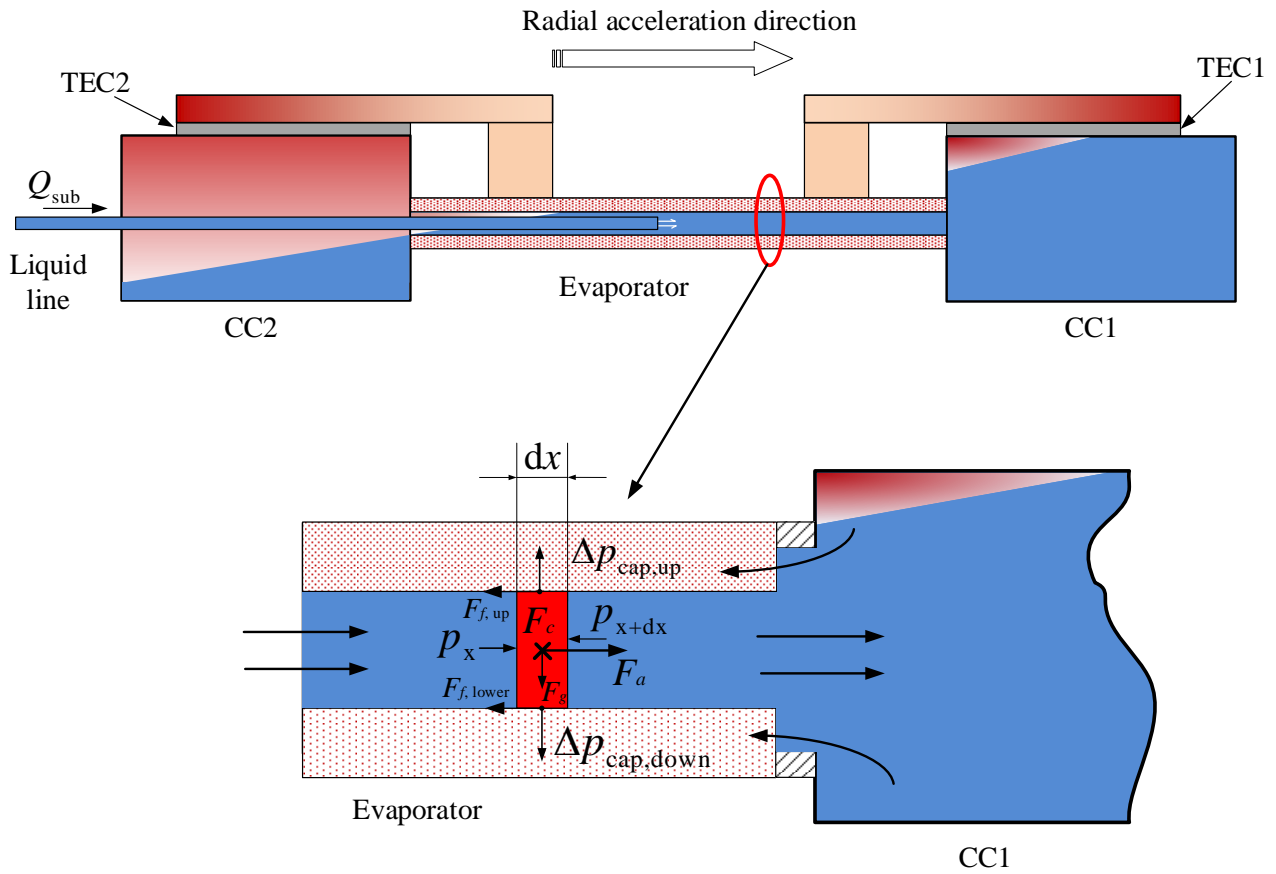
Fig. 6 presents the location sketch of 15 resistance temperature detectors (RTDs) on the DCCLHP. RTD1 and RTD2 are located on the upper and lower surface of the CC1. RTD3 is located at the middle of evaporator casing outer surface to monitor the evaporator temperature. RTD4 and RTD5 are placed on the upper and lower surface of the CC2, respectively. RTD6 and RTD7 are arranged at the inlet and outlet of the vapor line. RTD8-RTD11 are arranged on the condenser. While RTD12 and RTD13 are arranged at the inlet and outlet of the liquid line. RTD14 and RTD15 are used to measure the inlet and outlet temperatures of cooling water. RTD16 is used to monitor the ambient temperature.

### ***2.3. Experimental procedure***

Prior to the experiment, the calibration of the RTD is conducted in order to reduce the measurement error. At the beginning of the experiment, the cooling water circulation system is opened, and the cooling water temperature is controlled at 19 °C. Then turn on the signal measuring device to monitor the temperature of DCCLHP components and cooling water. When the water temperature reaches the constant, the load will be applied. During the experiment, the acceleration force and heat load on the evaporator are applied simultaneously. With the assistance of TEC, TEC starts simultaneously with the above two loads. If DCCLHP reaches a stable operating state within one hour, the acceleration force, TEC and heat load on the evaporator will be removed in turn. If the steady state has not been reached for nearly an hour or the evaporator temperature exceeds 60 °C, the TEC, acceleration force and heat load on the evaporator should be removed immediately.



(a) Under configuration A



(b) Under configuration B

**Fig. 5** Force analysis diagram of working fluid under two configurations

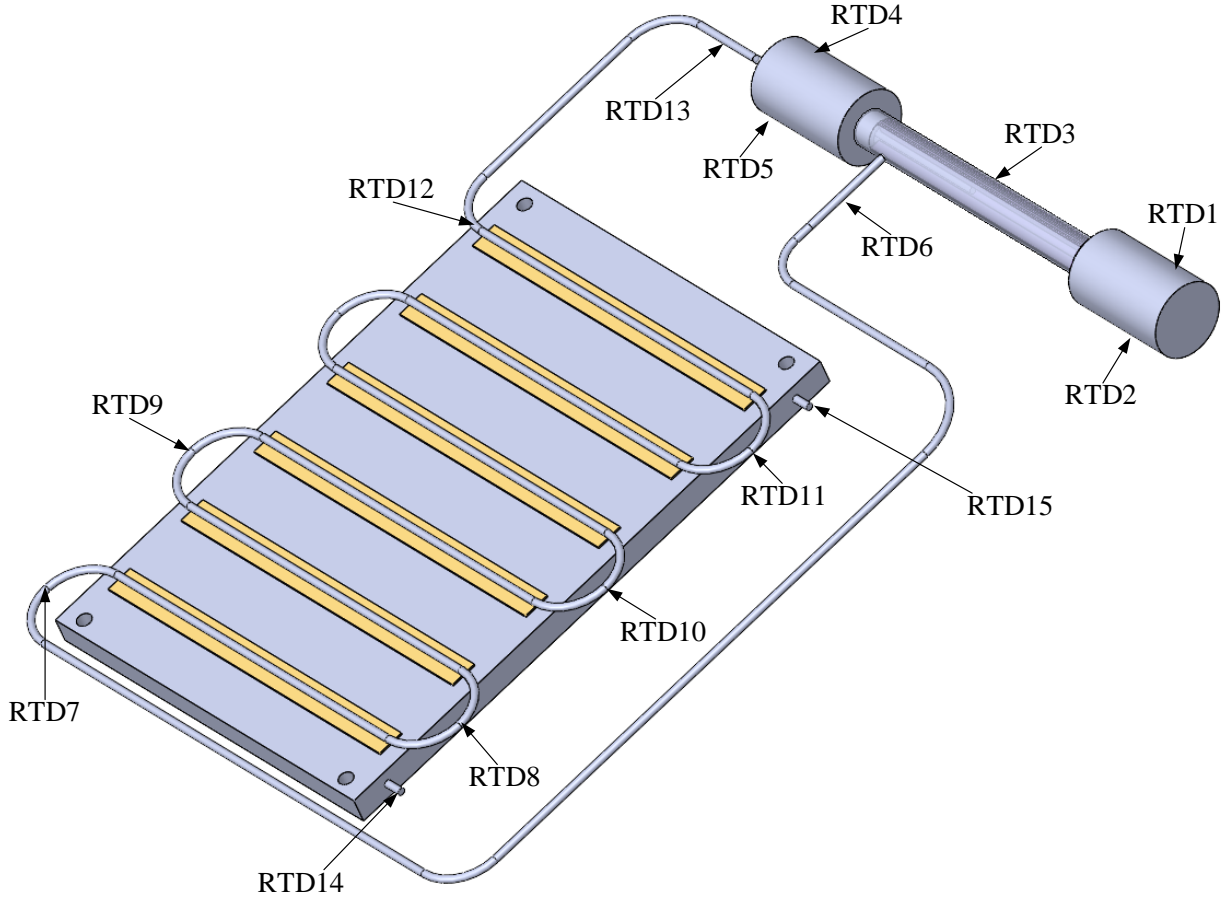


**Fig. 6.** The location sketch of RTDs on the DCCLHP.

#### 2.4. Thermal conductance calculation and Uncertainty analysis

Thermal conductance  $G$  reflects the heat transfer capability of a loop heat pipe, which is defined as

$$G = \frac{Q_e}{T_e - T_{\text{sink}}} \quad (1)$$

where  $Q_e$  is the heat load applied on the evaporator,  $T_e$  is the measured value of RTD3, and  $T_{\text{sink}}$  is the average of the measured values of RTD14 and RTD15. The thermal conductance of LHP is not a constant, it will be affected by heat load, acceleration, TEC and heat sink. At the same heat sink temperature, the larger the thermal conductance, the larger heat transfer capacity will be.

In the current work, the measurement accuracy of the Pt100 is  $\pm 0.3$  °C, but when the signal is transmitted in the electric slip ring, junction terminal, the collector and the long-distance electric wire, it could cause measurement accuracy to be  $\pm 0.5$  °C. The lowest temperature in the experiment is 18 °C, then the maximum uncertainty of temperature could be 2.8%.

The accuracy of the current  $I$  and voltage  $U$  in the heating power supply used in the experiment are 0.1 A and 0.1 V, while the minimum  $I$  and  $U$  are 1.31 A and 21 V. Therefore the maximum uncertainty of  $I$  and  $U$  are 7.6% and 0.48%, respectively. At the same time, considering the uncertainty caused by heat leakage to the environment and the uncertainty caused by  $I$  and  $U$ , the maximum uncertainty of the heat load is 5%. In summary, the uncertainty of each parameter is shown in Table 2

**Table 2** Uncertainty of the measurement

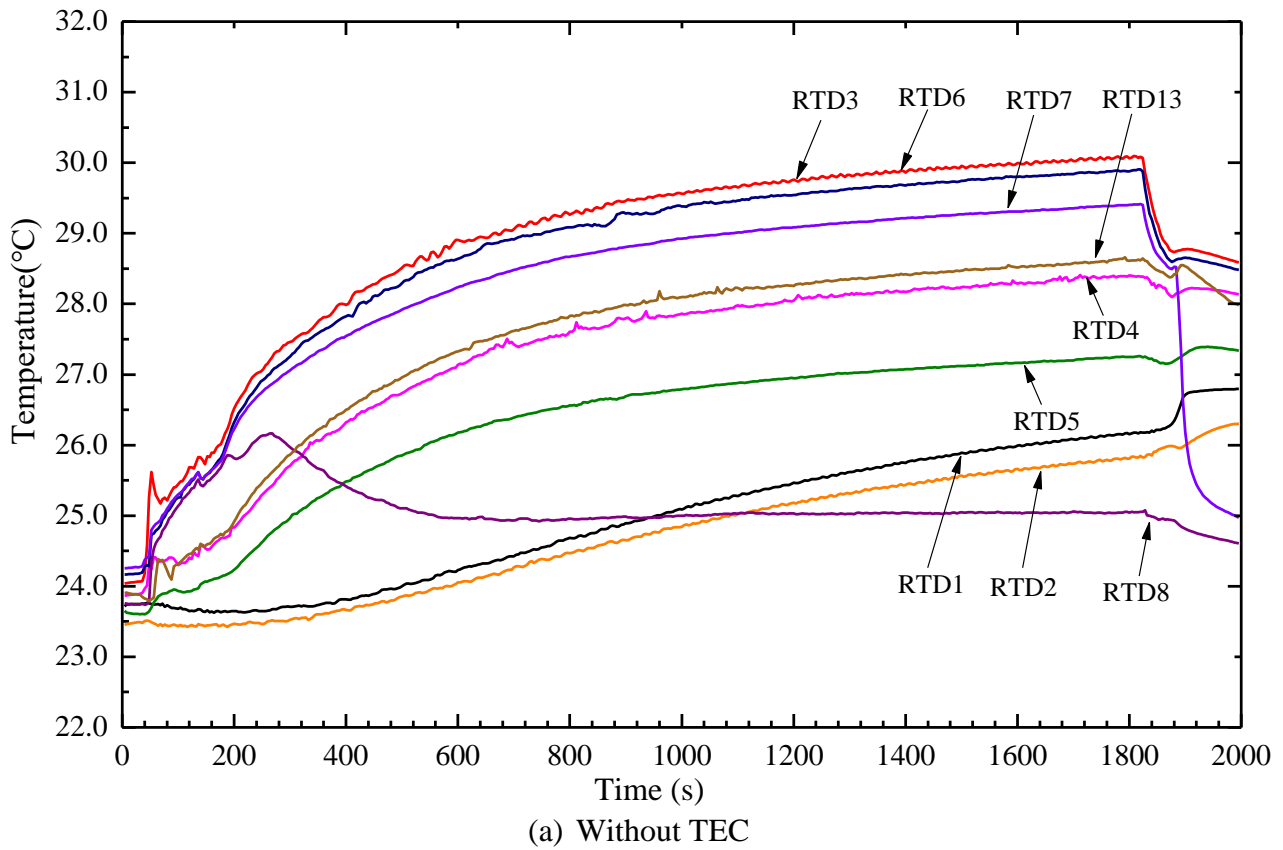
Parameter	Uncertainty
Temperature	2.8%
Current	7.6%
Voltage	0.48%
Heat load	5%

### 3. RESULTS AND DISCUSSION

The following sections mainly discuss the transient and steady-state performance of DCCLHP under various acceleration conditions. The influences of the TEC, acceleration magnitude and direction on the operating temperature and thermal conductance of the loop are analyzed in a systematic manner.

#### 3.1. Influence of TEC

The loop temperature profiles at 5 g with heat loads of 25 W under configuration B are plotted in Fig. 7. As can be seen from Fig. 7, the CC1 temperature is lower than that of CC2 no matter if the TEC is applied or not. When TEC is active, the CC1 temperature is 19.1 °C, whereas it is 26.1 °C when TEC is inactive.



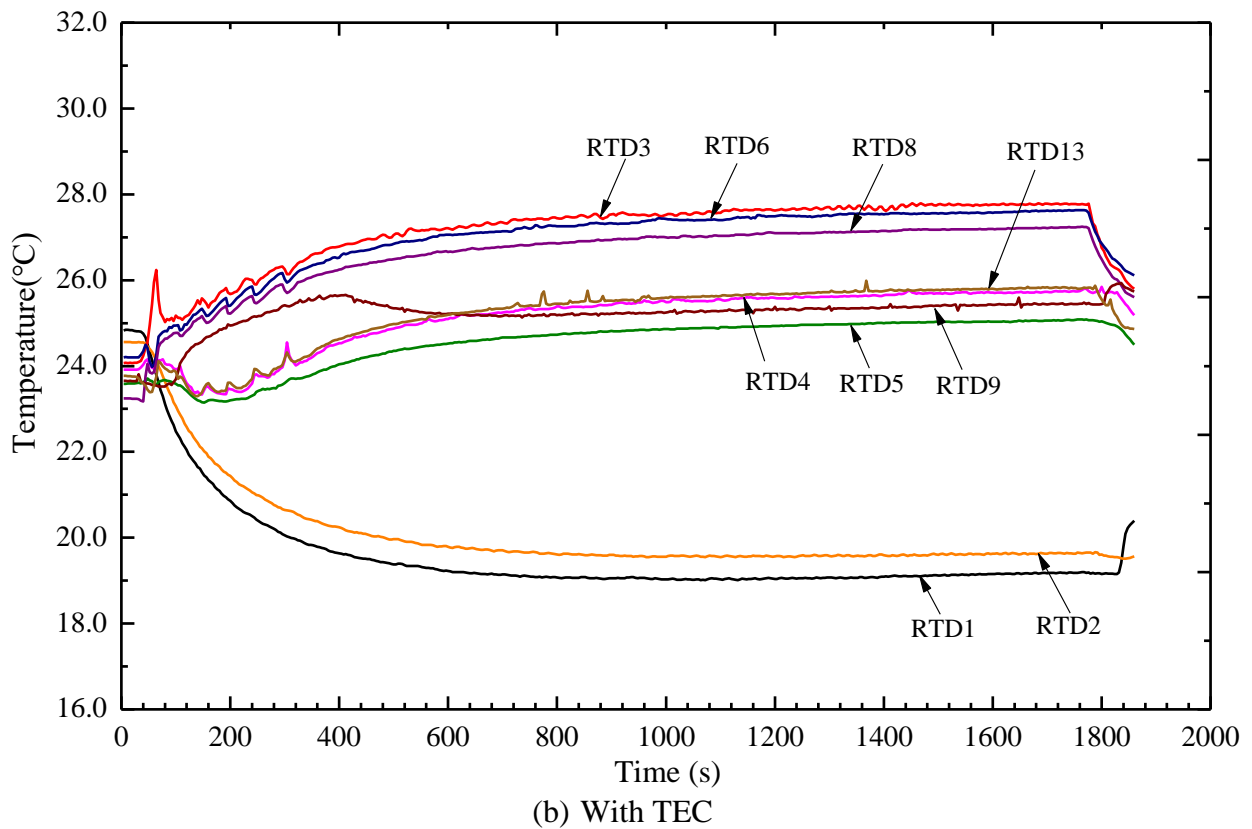


**Fig. 7.** Temperature profiles of the loop at 5 g and 25 W under configuration B.

As shown in Fig. 7(a), after the heat load is applied about 20 s, the evaporator immediately produces a temperature rise of 1.5 °C, and then the temperature decreases. At the same time, the temperature of RTD6 begins to rise which indicates that the vapor groove is full of liquid working fluid. It can also be observed from Fig 7(a) that the temperature of RTD7 and RTD8 increase with the temperature of RTD6 increases. It can be deduced that the vapor enters the vapor line, and the vapor-liquid interface moves to somewhere between RTD8 and RTD9. After the heat load is applied about 230 s, the RTD8 temperature on the condenser begins to decrease, which indicates that the vapor has retreated between RTD7 and RTD8. At about 1300 s, the evaporator temperature reaches a stable value of 30 °C. The temperature difference between the upper and lower surfaces of the CC1 and CC2 is 2.3 °C and 6.4 °C, respectively. It confirms that the liquid working fluid converges in CC1 under the influence of acceleration. Such vapor-liquid distribution in the evaporator and the CCs may result in greater heat leakage from the evaporator to the CC2 than to the CC1. Thus, the temperature of the CC2 is higher than that of the CC1.

From Fig. 7(b), the TEC enables the DCCLHP to operate at a lower temperature and shortens the time required to reach steady-state. With the TEC effect, the steady-state operating temperature of the evaporator is 27.5 °C, which is 2.5 °C lower than that without TEC. After applied the heat load for about 800 s, the DCCLHP reaches a stable operating state, and the vapor-liquid interface is between RTD8 and RTD9. The TEC plays an important role in two aspects: (1) to reduce the temperature of CCs, (2) to transfer heat from CCs to the evaporator. The transfer of heat from the hot side of TEC to the evaporator is equivalent to adding a certain amount of heat load. It can increase the rate of evaporation and thus generate more vapor which is also demonstrated by the fact that the vapor-liquid interface is pushed into somewhere between RTD8 and RTD9. The temperature of the CCs decreases, resulting in a decrease in internal pressure, which facilitates the return of liquid. The liquid reflux rate increases and the subcooled liquid returns to the evaporator, causing the evaporator temperature to decrease to a lower value.

As is known to all, the energy balance in the evaporator and the CCs decides the operating performance of the DCCLHP. The heat transfer between the CCs and the evaporator with TEC assisted is schematically presented in Fig. 8. When the DCCLHP operates at a steady state, the thermal equilibrium is established for the CCs and the evaporator. For the evaporator, the CC1 and the CC2, the energy balance equation can be written as Eqs (2), (3) and (4) respectively as the heat transfer with the ambient is negligible.

$$Q_e + Q_{TEC1, H} + Q_{TEC2, H} = Q_{leak1} + Q_{leak2} + Q_{sub, e} + Q_{evap} \quad (2)$$

$$Q_{leak1} = Q_{TEC1, L} + Q_{sub, 1} \quad (3)$$

$$Q_{leak2} = Q_{TEC2, L} + Q_{sub, 2} \quad (4)$$

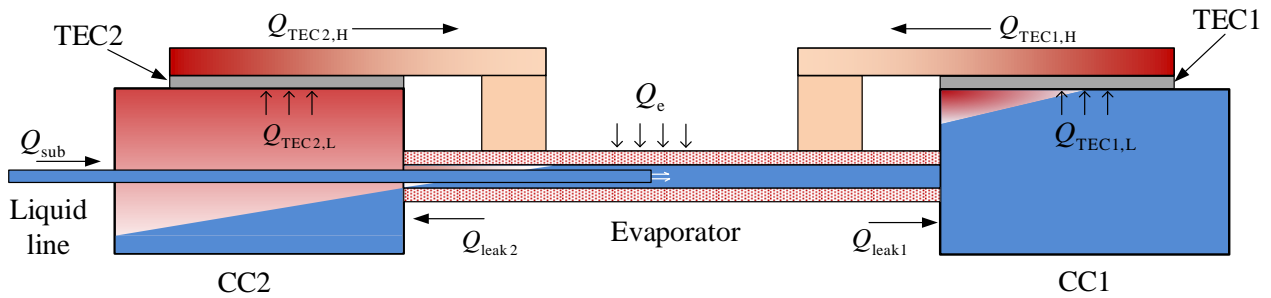
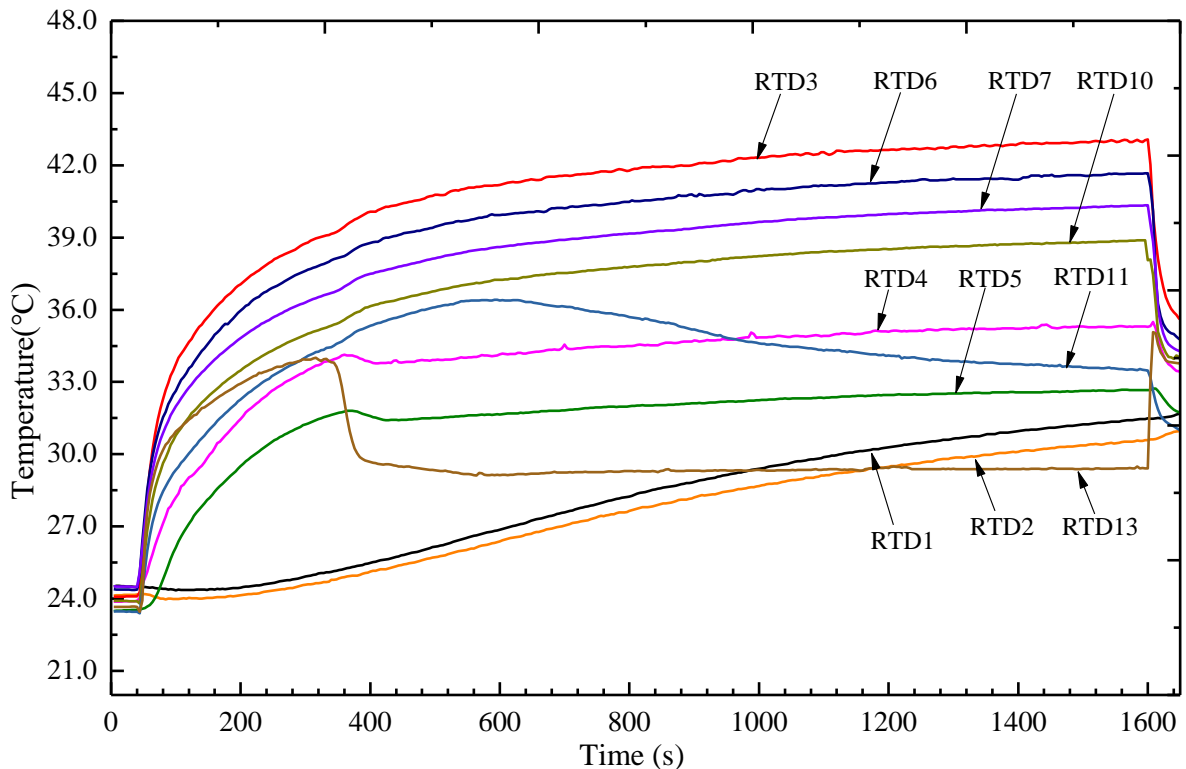


**Fig. 8.** Schematic diagram of heat transfer between CCs and evaporator.

Fig. 9 presents the temperature profiles of the DCCLHP at 5 g and 300 W under configuration B. As shown in Fig. 9, the biggest difference compared with the case at 25 W is that the evaporator temperature directly rises to a stable value. After the heat load is applied, the working fluid evaporates immediately, and a large amount of vapor is quickly entered into the vapor line. Therefore, the evaporator temperature rises immediately until it reaches a steady state.



(a) Without TEC

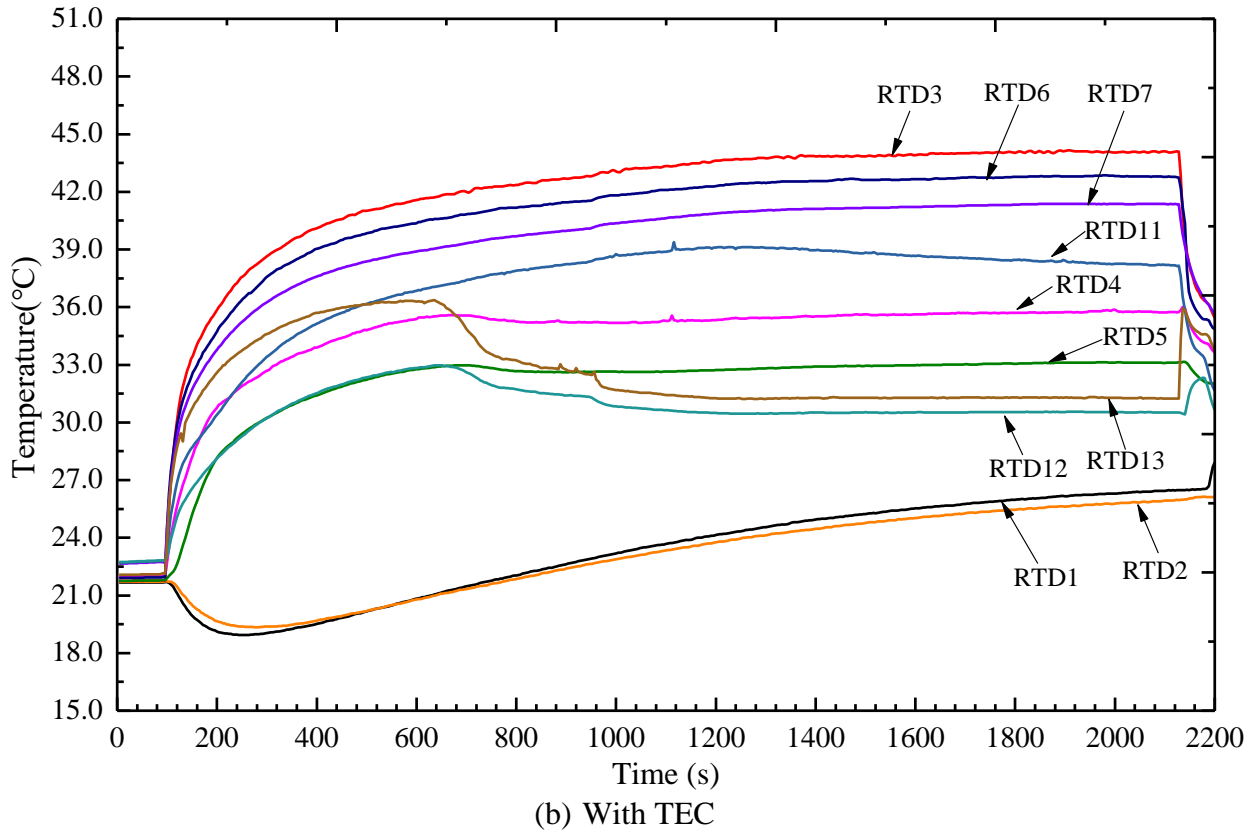
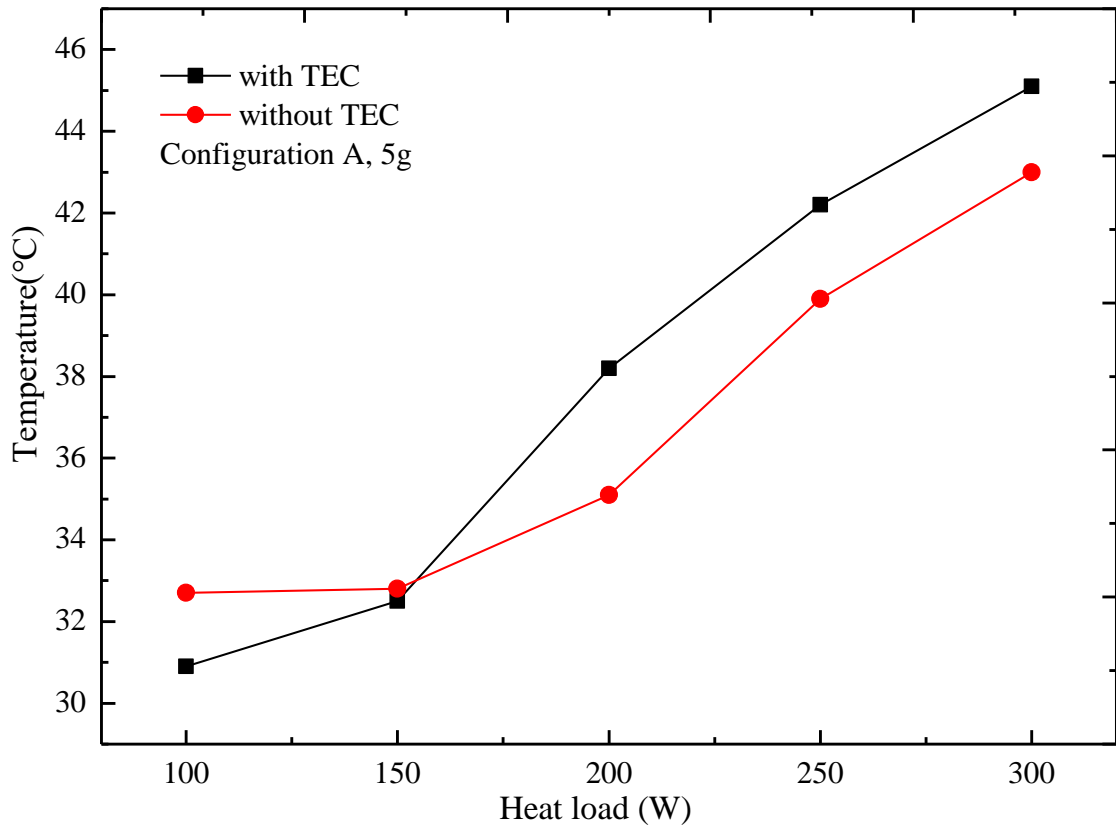


**Fig. 9.** Temperature profiles of the loop at 5 g and 300 W under configuration B.

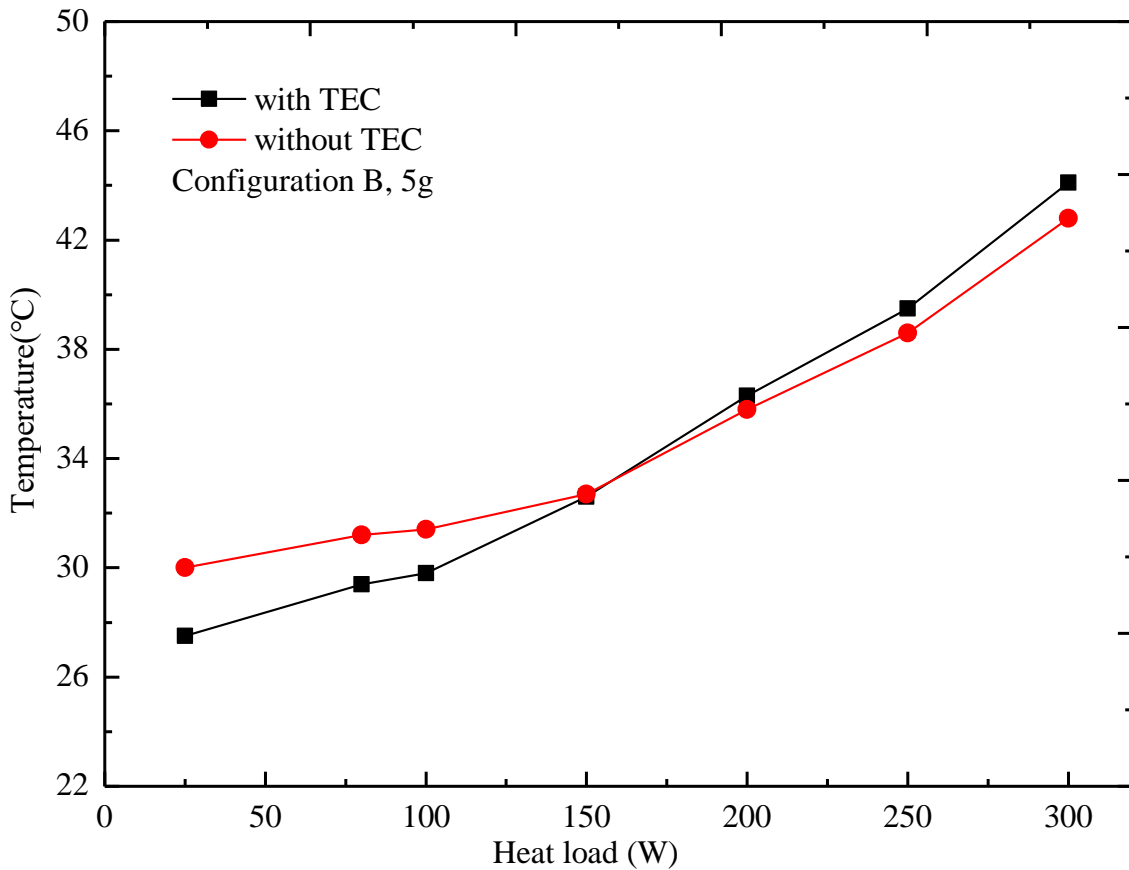
It can be seen from Fig. 9(a) that the DCCLHP reaches a steady-state after the heat load is applied about 1000 s. The evaporator temperature is 42.8 °C and the vapor-liquid interface is between RTD10 and RTD11. From Fig. 9(b), it can be observed that the DCCLHP reaches a stable operating state at about 1200 s. The evaporator temperature is 44.1 °C and the vapor-liquid interface is between RTD11 and RTD12. By comparing Fig. 9(a) and (b), it can be obtained that when the TEC is applied, the temperature of the CC is lower than that without TEC, and the effective condensation length of the condenser is further expanded, but the trend of the evaporator temperature change is almost the same. For a fixed TEC power, its heat transfer capacity is related to the temperature difference between the hot side and the cold side. The larger the temperature difference between the two sides of the TEC, the smaller the heat transferred by it. At the heat load of 300 W, higher evaporator temperature could lead to not only a larger heat leak from the evaporator to the CCs, but also a larger temperature difference between both sides of TEC. The large temperature difference between the evaporator and CCs could result in low cooling effect although the heat could be transferred from the CCs to evaporator through the thermal bridge. Consequently, the temperature of both RTD1 and RTD2 increases gradually.

Fig. 10 shows the operating temperature and thermal conductance versus heat load for the case of 5 g with and without TEC under both configurations A and B. Under configuration A, when the heat load is 100 W, TEC reduce the evaporator temperature by 1.5 °C and increase the thermal conductance by 9 W/K. When the heat load is 150 W, the steady operating temperature and the thermal conductance with TEC are substantially equal to that without TEC. When the heat load is larger than 150 W, TEC leads to the operating temperature to increase and thermal conductance to decrease. Under configuration B, when the heat load is 150 W, the steady operating temperature with TEC is equal to that without TEC, both of which are 32.5 °C. When the heat load is in the range of 200 ~ 300 W, the application of TEC will increase the operating temperature and decrease the thermal conductance slightly. When the heat load is in the range of 25 ~ 100 W, the application of TEC can reduce the operating temperature and increase the thermal conductance significantly. It can be

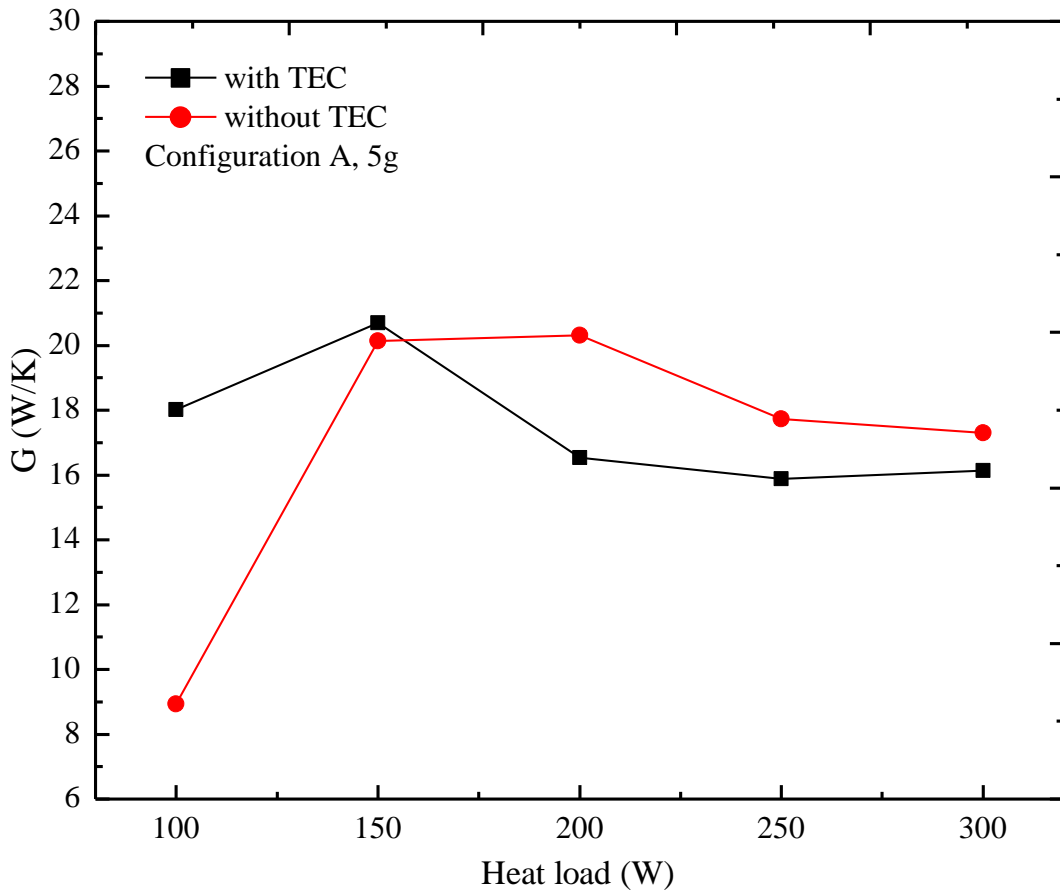
concluded from Fig. 10 that TEC only assists the operation of DCCLHP at small heat loads under both two configurations. The threshold heat load that TEC worsens the operating performance of the loop under configurations A and B is 150W and 100W respectively.



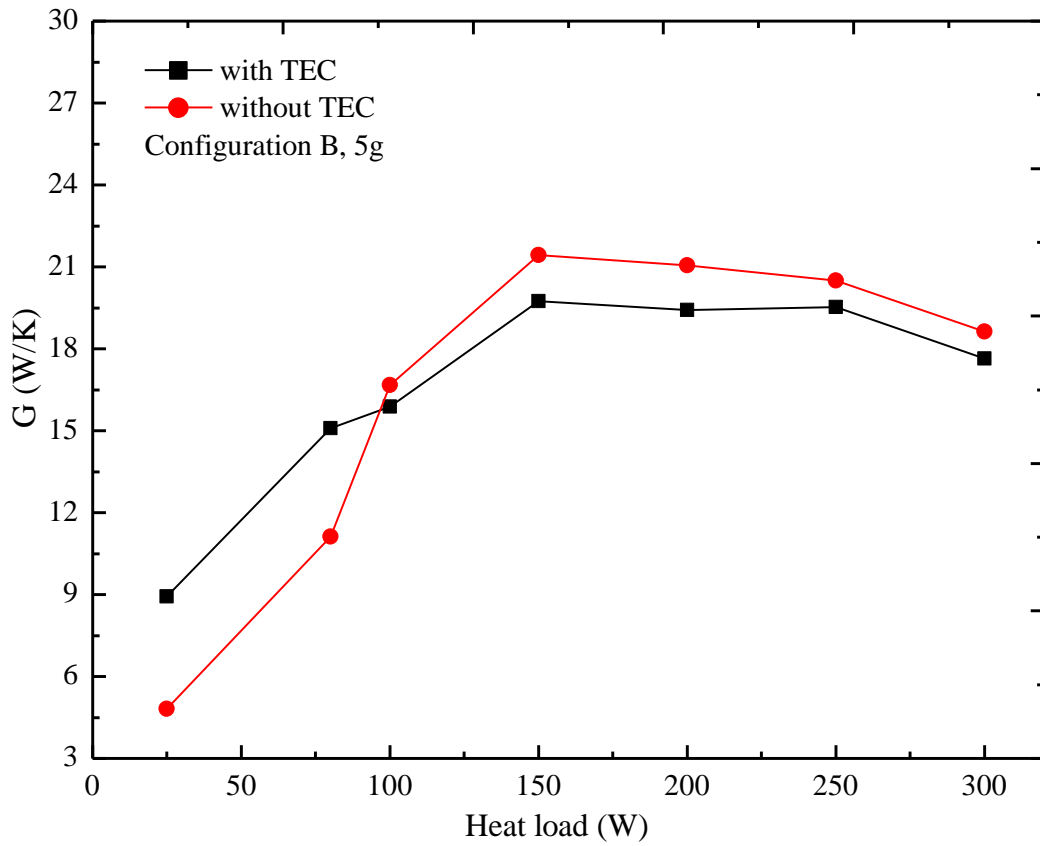
(a) Operating temperature under configuration A



(b) Operating temperature under configuration B



(c) Thermal conductance under configuration A



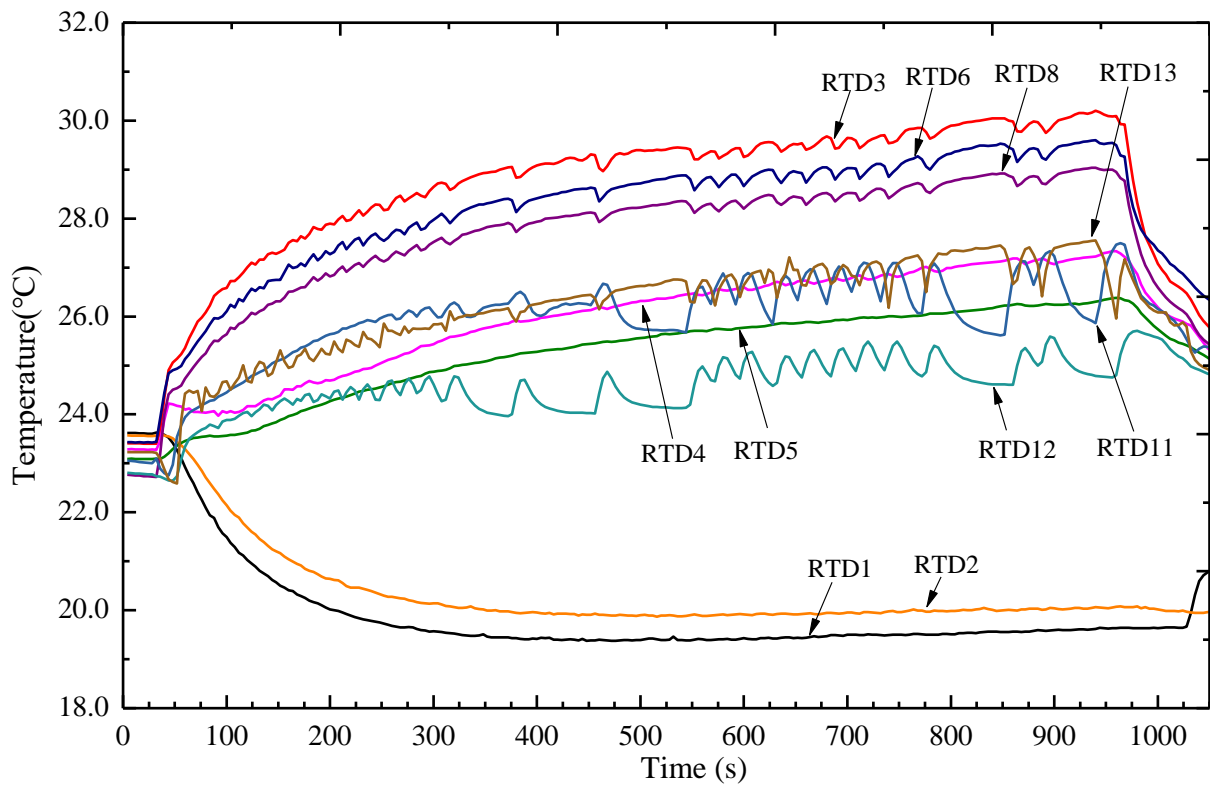
(d) Thermal conductance under configuration B

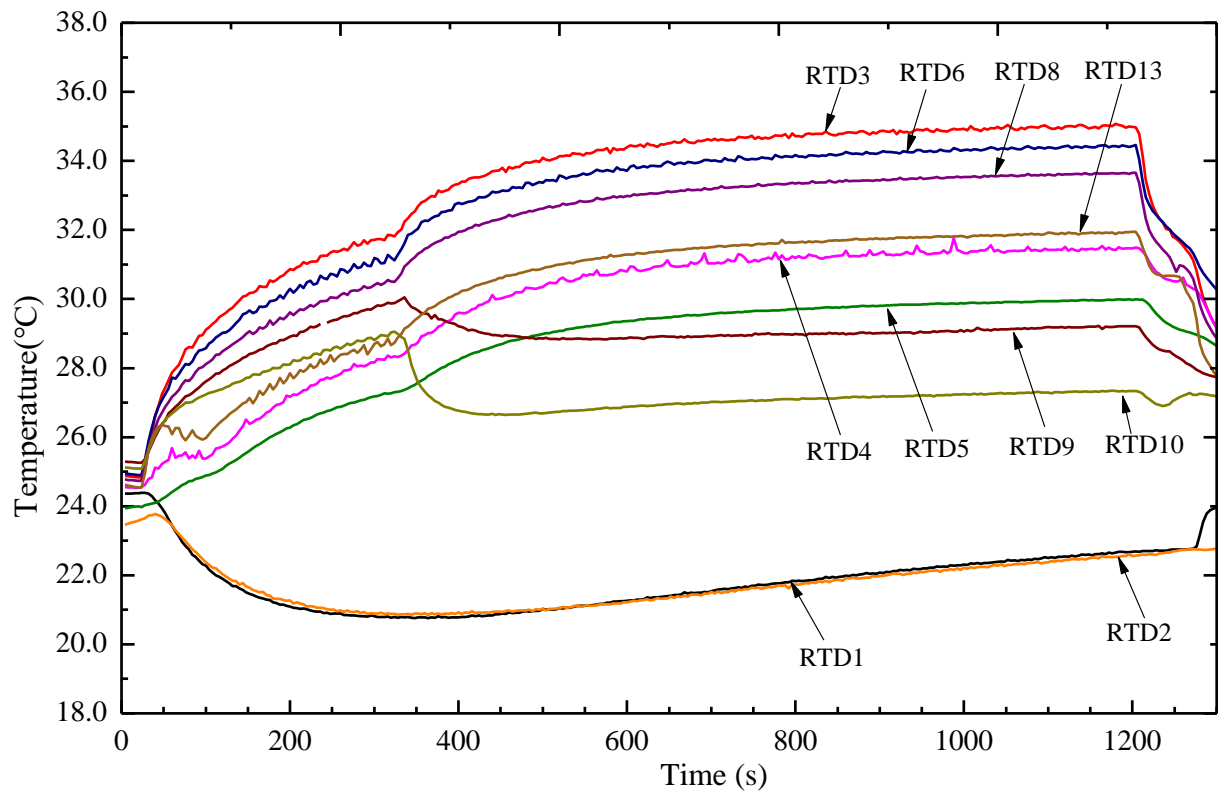
**Fig. 10.** Operating characteristics versus heat load for cases at 5 g with and without TEC.

### 3.2. Influence of acceleration magnitude

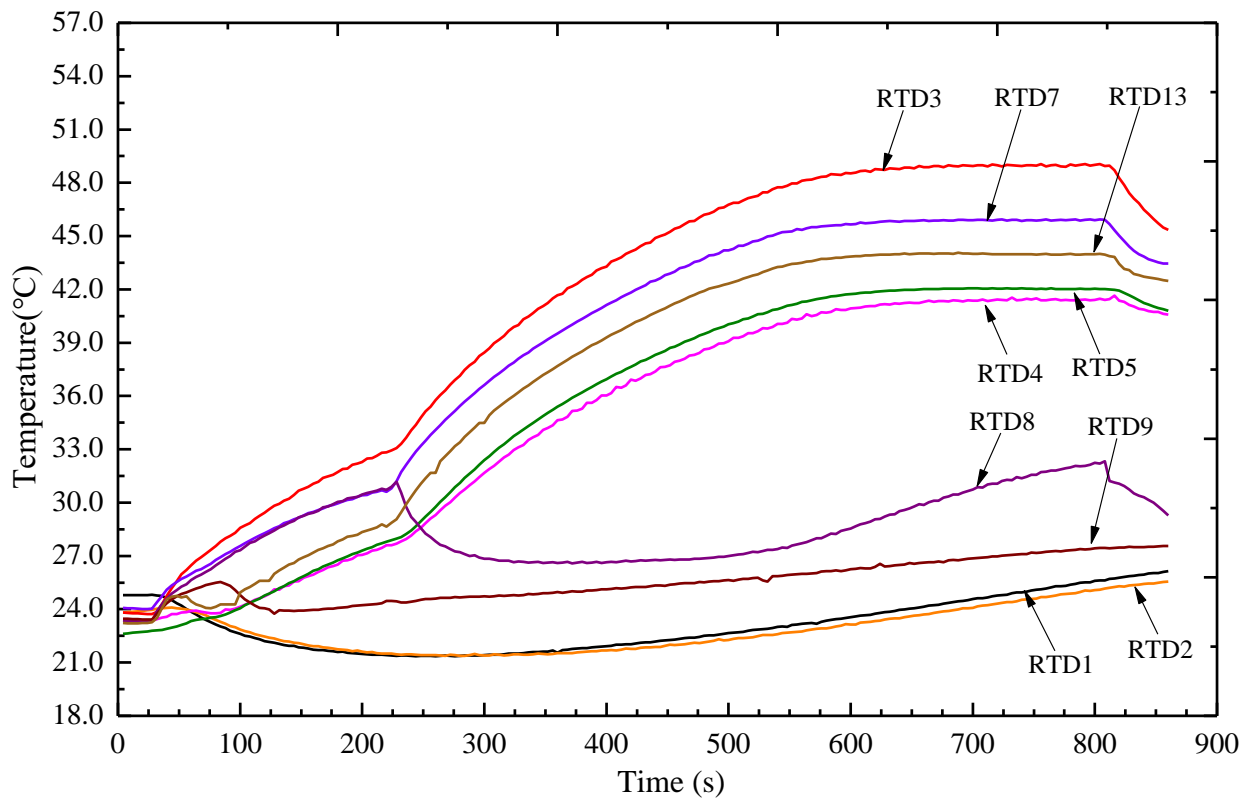
The experimental results show that when DCCLHP is arranged at configurations A and B, the acceleration varies from 5 g-13 g, and the heat load range is 25-300 W, it can successfully start up with the assistance of TEC. It is worth noting that the operating performance of DCCLHP is not significantly affected by the acceleration under configuration A except for the case of 150 W. It could be the reason that the acceleration has little effect on the vapor-liquid distribution in the loop and the external loop pressure drop. Therefore, the effect of acceleration magnitude on DCCLHP under configuration B will be discussed here only.

Fig. 11 presents the temperature curve of DCCLHP under different acceleration magnitudes for the case of configuration B with TEC when the heat load is 100 W. In the current study, periodic temperature fluctuation phenomenon is observed at 5 g and 7 g. But the loop does not show temperature fluctuation at 13 g. The maximum operating temperature of the DCCLHP at 5 g, 7 g and 13 g is 30.2 °C, 35 °C and 48.8 °C, respectively.





(b) 7 g



(c) 13 g

**Fig. 11.** Temperature profiles with TEC at 100 W and configuration B under 5 g, 7 g and 13 g.

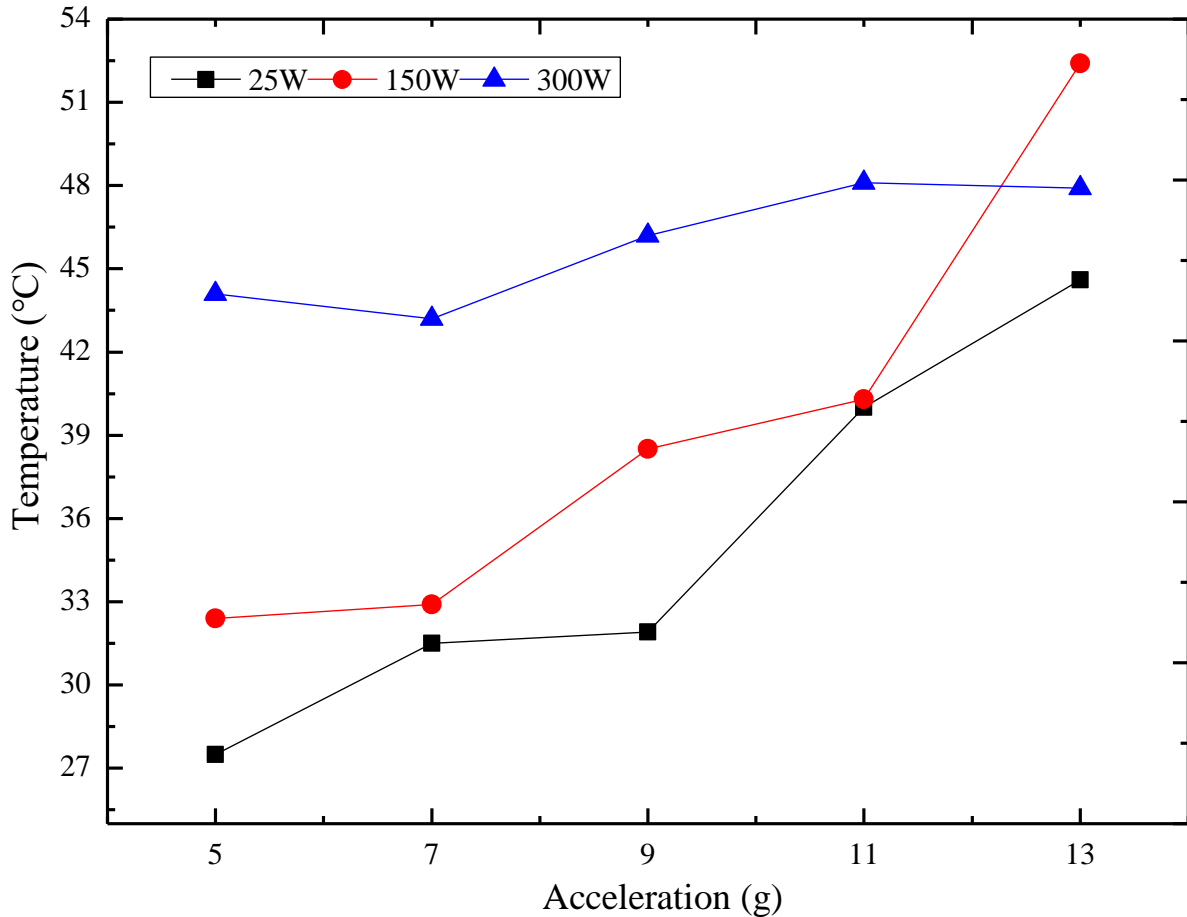
As can be seen from Fig. 11(a), after the acceleration is applied at about 30 s, the liquid with the lower temperature from the condenser enters into the liquid line which causes the RTD12 and RTD13 temperature drop. Then the temperature of RTD12 and RTD13 rises rapidly due to the subcooling of

the returning liquid decrease by the condensation length increase. At about 70 s, the RTD13 temperature begins to fluctuate upward with a period of 18 s. Then the temperature of the evaporator, the vapor line and the condenser also begins to fluctuate slightly after about 90 s. However, after about 320 s, the period of temperature fluctuation of the loop increases to approximate 81 s suddenly. The amplitude of RTD12 and RTD3 increases to around 1.0 °C and 0.5 °C. At about 550 s, the temperature fluctuation begins to decrease its period to 27 s. The temperature fluctuation with varying period sustains to the test end. It is difficult to explain the reason how the type of periodic temperature fluctuation of the loop occurs. But it can be confirmed that the acceleration effect and the instability of the two-phase flow play an important role. Finally, the evaporator temperature ranges from 29.7 °C to 30.2 °C at a quasi-steady state. During the whole process, the temperature of CC1 and CC2 does not fluctuate due to the effect of TEC. The temperature difference between the upper and lower surfaces of the CC1 and the CC2 is approximate 0.5 °C and 1.0 °C, respectively.

In Fig. 11(b), the variation of the loop temperature at 7 g is similar to that shown in Fig. 11(a) before around 330 s. A slight temperature fluctuation occurs on the evaporator, condenser, the vapor line and liquid line. After about 330 s, the vapor-liquid interface moves to somewhere between RTD8 and RTD9 according to the condenser temperature. The condensation length reduces and the subcooling of the returning liquid increases. In the meantime, the pressure drop of the external loop resulted from the acceleration force increases. The heat leak from the evaporator to CCs also increases. As a result, the evaporator temperature rises and the temperature fluctuation of the loop disappears quickly. Finally, the DCCLHP gets to a steady state and the operating temperature is 35 °C. The temperature of the upper and lower surface of the CC1 is almost identical. While the temperature difference between the upper and lower surface of the CC2 is enlarged to 1.5 °C. The reason can be explained as follows. With the increase of the acceleration, more liquid working fluid is pushed into the CC1 and the vapor enters into the CC2. Moreover, the decrease of the condensation length makes the liquid in the CCs be substituted into the condenser. It causes more vapor to occupy the CC2. Due to the liquid has a larger heat capacity than the vapor, the temperature difference of the CC1 is very small by the effect of TEC. While the CC2 has a large temperature difference.

When the acceleration increases to 13 g shown in Fig. 11(c), the temperature of the evaporator, the vapor line and the CC2 rises and the CC1 temperature drops slowly before about 80 s. Then the RTD9 temperature begins to drop which indicates the vapor-liquid interface moves to somewhere between RTD8 and RTD9. At around 229 s, the RTD8 temperature also decreases. According to the temperature of RTD7, RTD8 and RTD9, it is recognized that the vapor-liquid interface gradually moves to somewhere near RTD7 between RTD7 and RTD8 before about 500 s. At about 800 s, the evaporator temperature increases to a constant value of 48.8 °C. The interface locates somewhere near RTD8. The reason behind the above temperature changes can be explained as follows. Under the effect of the acceleration, on the one hand, the CC1 is nearly filled with the liquid and the CC2 is almost full of the vapor. Thus, the heat leak from the evaporator to the CC2 increases, which is larger than that to the CC1. The CC2 temperature is significantly larger than the CC1 temperature imposed additionally by the TEC cooling. When the working fluid in the CCs is displaced into the condenser, some bubbles could be generated in the core and reversely flow into the liquid line through the bayonet. Afterwards, they may stagnate near RTD13 which leads to a higher temperature of the RTD13. On the other hand, the movement of the vapor-liquid interface changes the condensation length and the pressure drop of the external loop. As the interface moves from RTD7 to RTD8, the pressure drop resulted from the acceleration force will increase because of the effective liquid length increasing. According to the Clausius-Clapeyron equation, the evaporator temperature rises to provide enough capillary force for the pressure balance of the loop. Finally, the DCCLHP reaches a steady state. The temperature difference between the upper and lower surfaces of CC2 is less than 0.5 °C, whereas the temperature is almost kept constant in the CC1.

Fig. 12 presents the stable operating temperature and thermal conductance of the DCCLHP with TEC versus acceleration magnitude under configuration B at three different heat loads of 25 W, 150 W and 300 W. As shown in Fig. 12(a), for the case of 25 W, the operating temperature was 27.5 °C, 31.5 °C, 31.9 °C, 42.0 °C, 44.6 °C at 5 g, 7 g, 9 g, 11 g, and 13 g, respectively. At 150 W, the operating temperature was 32.4 °C, 32.9 °C, 38.5 °C, 40.3 °C, 52.4 °C at 5 g, 7 g, 9 g, 11 g, and 13 g respectively. At 300 W, the operating temperature was 44.1 °C, 43.2 °C, 46.2 °C, 48.1 °C, 47.9 °C at 5 g, 7 g, 9 g, 11 g, and 13 g respectively. It can be concluded that, at a small heat load of 25 W and 150 W, the steady-state operating temperature with TEC increases with the acceleration increasing. Under the large heat load of 300 W, the acceleration has an insignificant effect on the steady operating temperature. In addition, it should be noted that the operating temperature at 13 g and 150 W is obviously higher than that at 300 W and 13 g. The reason could refer to the above description of the case of 100 W shown in Fig. 11(c).



(a) Operating temperature

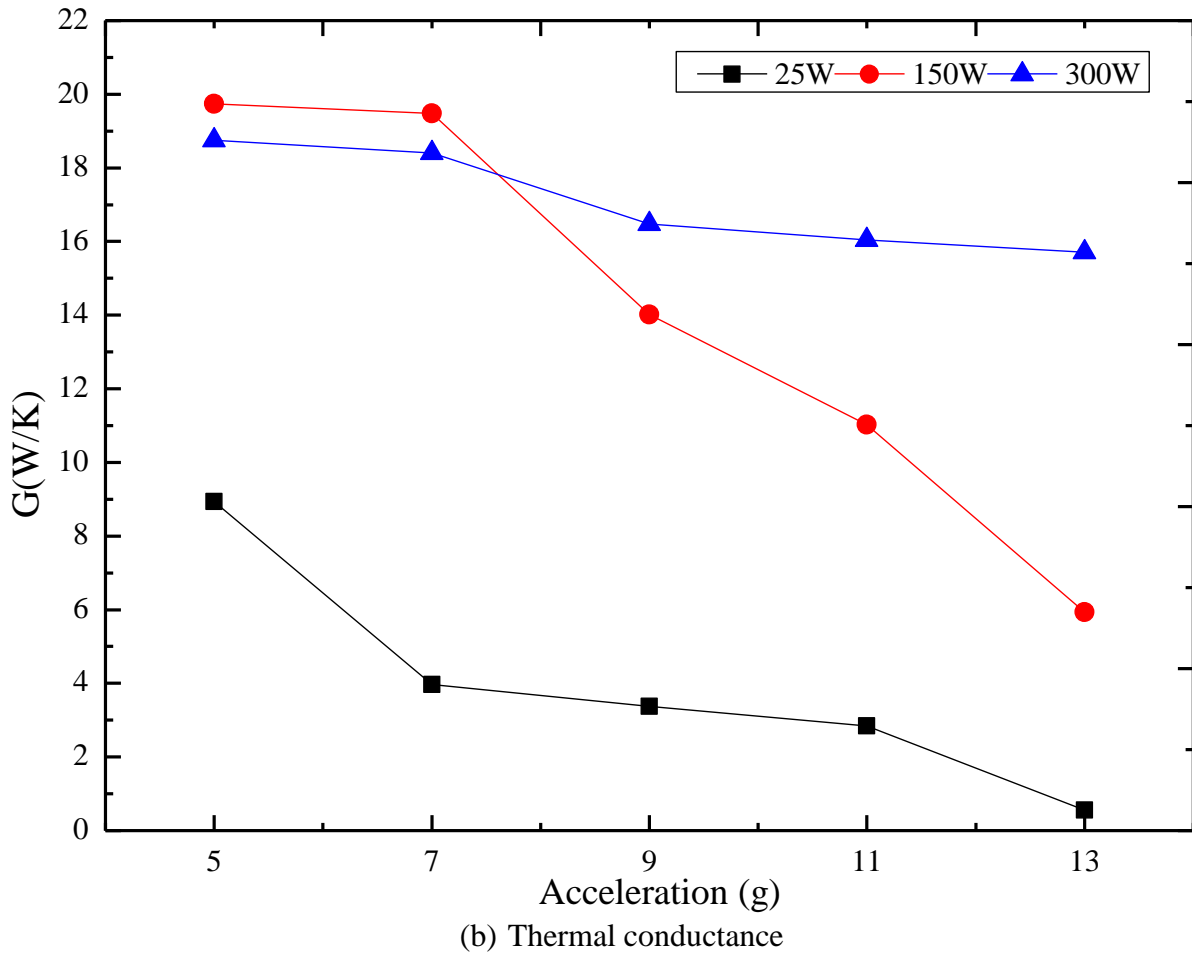


**Fig. 12.** Operating characteristics versus acceleration magnitude for cases with TEC under configuration B at 25 W, 150 W and 300 W.

In Fig. 12(b), it can be clearly seen that the variation of thermal conductance versus acceleration magnitude shows an opposite trend with that of operating temperature. The higher the acceleration magnitude, the lower the thermal conductance. At 25 W, the thermal conductance is 8.93 W/K, 3.97 W/K, 3.38 W/K, 2.84 W/K and 0.56 W/K at 5 g, 7 g, 9 g, 11 g and 13 g respectively. It is significant less than that at 150 W and 300 W. When the heat load is 150 W, the thermal conductance is 19.74 W/K, 19.48 W/K, 14.02 W/K, 11.03 W/K and 5.93 W/K at 5 g, 7 g, 9 g, 11 g and 13 g respectively. When the heat load is 300 W, the thermal conductance is 18.75 W/K, 18.4 W/K, 16.48 W/K, 16.04 W/K and 15.71 W/K at 5 g, 7 g, 9 g, 11 g and 13 g respectively. In addition, for a small heat load, the acceleration magnitude significantly affects the operating temperature and thermal conductance. While for a large heat load, the influence of the acceleration magnitude is not obvious on the operating temperature and thermal conductance.

### 3.3. Influence of acceleration direction

Fig. 13 shows the temperature profiles of the DCCLHP with TEC at 5 g under configuration A as the heat load is 100 W and 300 W. It can be found from Fig. 13 that the evaporator and the CCs present similar trend of temperature rise. The DCCLHP reaches to a steady state finally.

It can be found from Fig. 11(a) and Fig. 13(a) that the most significant difference is that there is no temperature fluctuation. Under configuration A, the direction of the acceleration force is perpendicular to the axis of the evaporator, which has an insignificant impact on the distribution of the working fluid in the evaporator and the CCs. In Fig. 13(a), the upper surface temperature of the

CC1 and the CC2 is 25 °C and 25.2 °C respectively. It represents that the vapor-liquid distribution in both CCs may be identical approximately. When the DCCLHP operates to a steady state, the evaporator temperature is 31 °C, which is an increase of 1.5 °C compared to that of configuration B shown in Fig. 11(a).

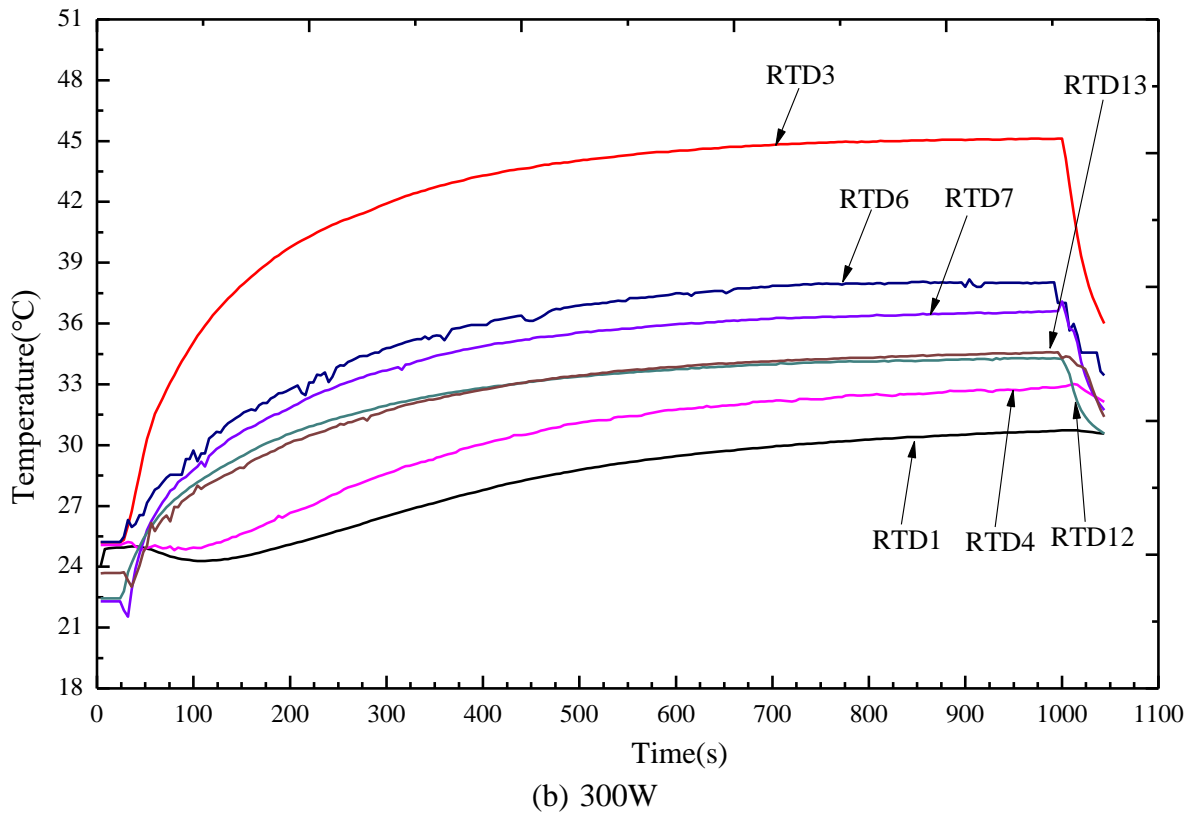
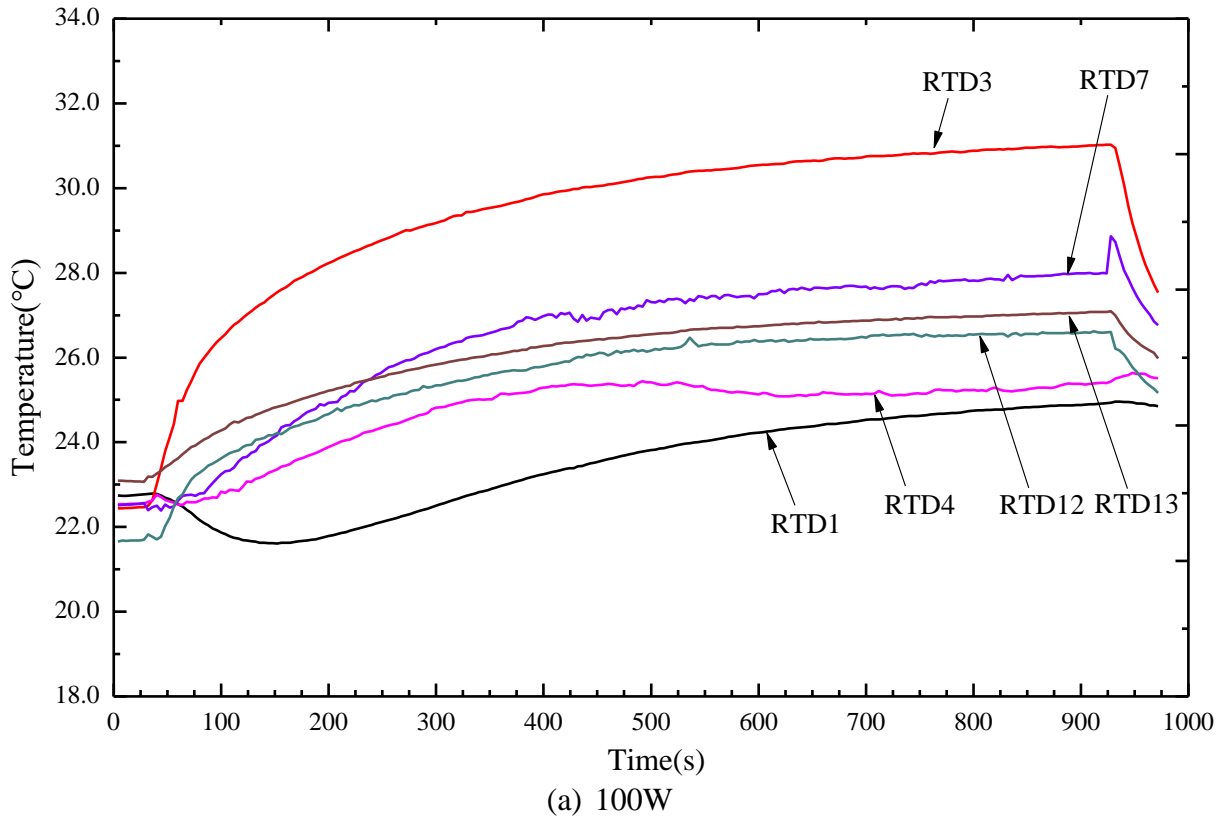
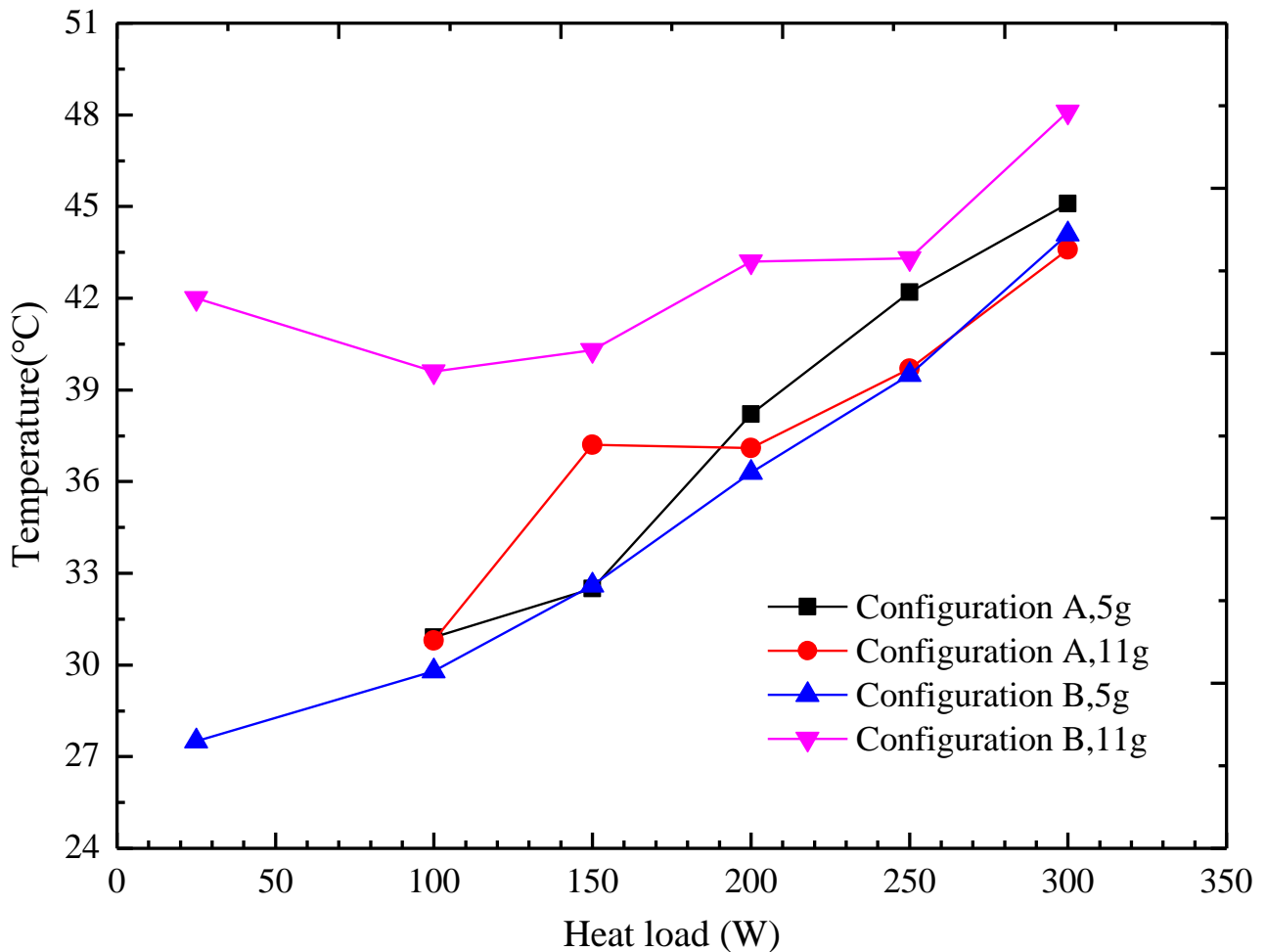


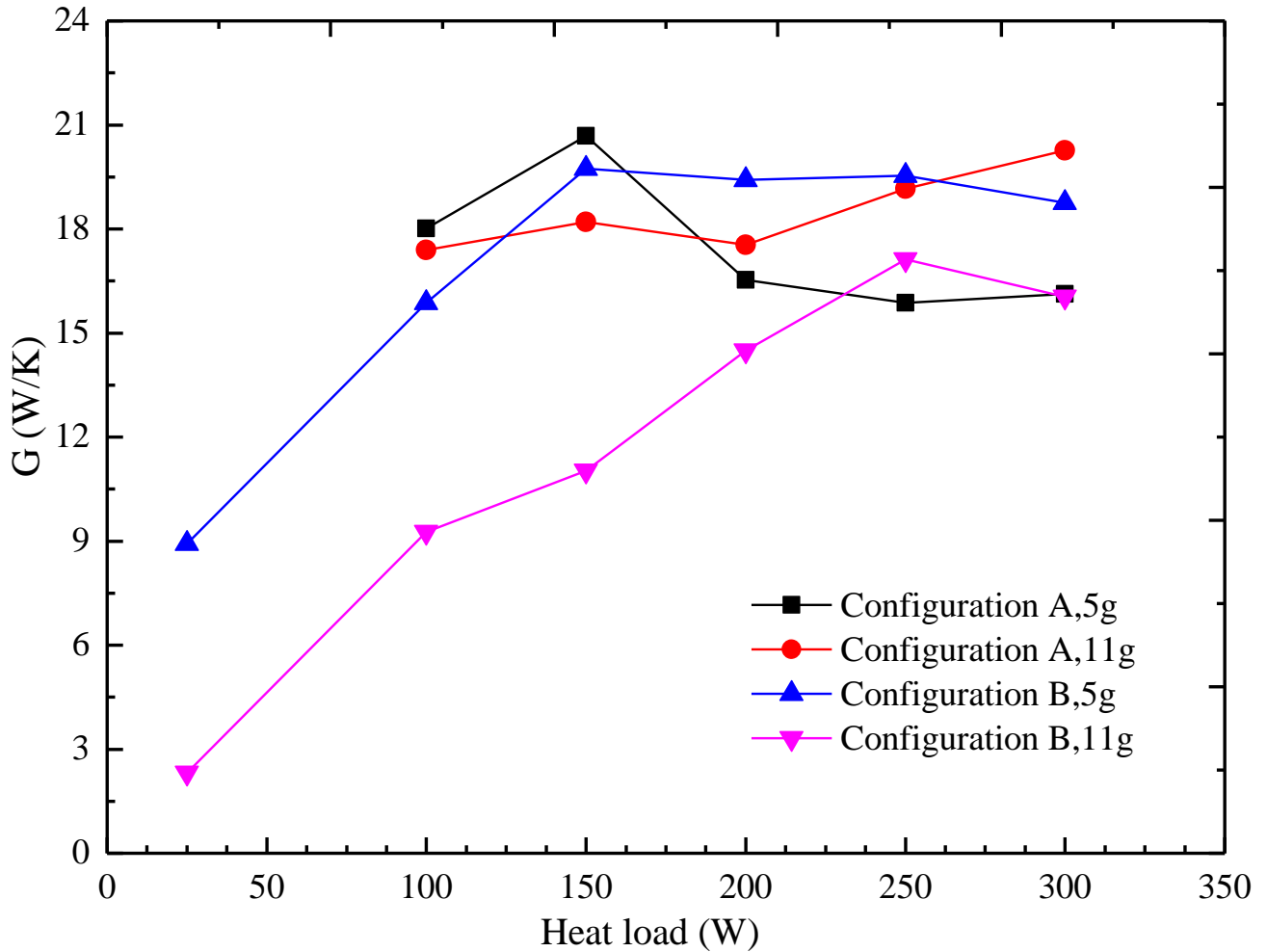
**Fig. 13.** Temperature profile with TEC for cases of 100 W and 300 W at 5 g under configuration A.

In Fig. 13 (b), after the heat load and acceleration are applied, the RTD7 temperature decreases initially. This could be explained by the fact that the liquid in the condenser moves back into the vapor line under the effect of inertia. Along with the evaporation occurring in the evaporator, the vapor immediately entered into the vapor line and the condenser. The RTD7 temperature starts to increase again. When the entire loop achieves the steady state, the evaporator temperature is 45.1 °C. The temperatures of the CC1 and the CC2 is 30.5 °C and 32.7 °C, respectively. Compared with that under configuration B, as shown in Fig. 9(b), the loop reaches a steady state within a shorter time of about 500 s. The operating temperature in Fig. 13(b) increases by about 1.0 °C. The temperature difference between the CC1 and the CC2 decreases to 2.0 °C.

Fig. 14 presents the operating temperature and thermal conductance with TEC at 5 g and 11 g under both configurations A and B. As is obviously observed from Fig. 14, for the case of 5 g, the operating temperature under configuration A is higher than that under configuration B. The thermal conductance at 25 W, 100 W and 150 W under configuration A is less than that under configuration B. While for the case of 11 g, the operating temperature under configuration A is significantly less than that under configuration B. The thermal conductance under configuration A is obviously higher than that under configuration B.



(a) Operating temperature



(b) Thermal conductance

**Fig. 14.** Operating temperature and thermal conductance versus heat load with TEC at 5 g and 11 g under both configurations A and B.

In Fig. 14(a), at 300 W and 5 g, the operating temperature under configurations A and B is 45.1 °C and 44.1 °C. While at 300 W and 11 g, the operating temperature under configurations A and B is 43.6 °C and 48.1 °C, respectively. At 100 W and 5 g, the operating temperature is 30.9 °C and 29.8 °C under both configurations A and B respectively. But at 100 W and 11 g, the operating temperature is 30.8 °C and 39.6 °C, respectively. Under configuration B, the operating temperature difference between 5 g and 11 g decreases with the heat load increase gradually. While under configuration A, the operating temperature difference shows a small variation with the heat load increase except for the case of 150 W.

In Fig.14(b), under configuration A, the minimum and maximum thermal conductance at 5 g and 11 g are 15.9 W/K and 20.7 W/K, respectively. While the minimum and maximum value at 5 g and 11 g are 2.3 W/K and 19.7 W/K under configuration B. At 300 W and 5 g, the thermal conductance is 16.1 W/K and 18.3 W/K under configurations A and B, respectively. At 300 W and 11 g, the thermal conductance is 20.3 W/K and 16.0 W/K under configurations A and B, respectively. When the heat load is more than 200 W, the thermal conductance change is small relative to that as the heat load is less than 200 W.

## 4. CONCLUSIONS

In this work, the effect of different heat loads, acceleration magnitudes and directions on the operating performances of a stainless steel-ammonia DCCLHP integrated with TEC under acceleration fields were studied by experiment. The main conclusions can be summarized as follows:

- (1) At 100 W and 150 W under configuration A, TEC with the power of 10 W can decrease operating temperature with the maximum value of 1.8 °C and increase thermal conductance with the maximum value of 9.1 W/K, but it has adverse effect at 150 W, 200 W and 300 W. Under configuration B, TEC can decrease operating temperature with the maximum value of 2.5 °C and increase thermal conductance with the maximum value of 4.2 W/K in the range of 25 W-150 W. but it has adverse effect at the range of 100 W-300 W.
- (2) Generally, the operating temperature with TEC increases with the acceleration increase under configuration B. While the thermal conductance reduces with the acceleration increase. Under configuration A, the operating performance is not significantly affected by the acceleration for most cases. The maximum and minimum operating temperature is 56.7 °C at 150 W under 13 g and 27.6 °C at 25 W under 5 g for configuration B. The maximum and minimum thermal conductance is 20.7 W/K at 150 W under 5 g for configuration A and 0.6 W/K at 25 W under 13 g for configuration B.
- (3) A visible temperature fluctuation is observed at 100 W under 5 g and 7 g for configuration B. The temperature fluctuation disappears under 13 g. While no temperature fluctuation occurs under configuration A. Furthermore, the time that reaches the steady state under configuration A is shorter than that under configuration B at the same heat load and acceleration.
- (4) The operating characteristics of the DCCLHP under acceleration conditions are the result of the comprehensive effects of heat load, acceleration magnitude and direction as well as TEC. The vapor-liquid distribution in the loop and pressure drop of the external loop can be altered by the acceleration effect. The CCs that cooled by the TEC can contribute to reduction of the operating temperature.

## ACKNOWLEDGMENT

The authors acknowledge the financial supports from National Natural Science Foundation of China (No. 11772038).

## NOMENCLATURE

$g$	Gravitational acceleration	[9.81 m/s <sup>2</sup> ]
$G$	Thermal conductance	[W/K]
$Q$	Heat load	[W]
$T$	Temperature	[K]
$I$	Current of heating power supply	[A]
$U$	Voltage of heating power supply	[V]
$p$	Pressure	[Pa]
$F$	Force	[N]
$\Delta p$	Capillary force	[N]

### *Subscripts*

e	Evaporator
in	At inlet
out	At outlet

sink	Heat sink
evap	Evaporation
sub	Subcooled liquid fluid
$x$	Position at the evaporator core
$a$	Acceleration
$c$	Coriolis
cap, up	Upper surface capillary force
cap, lower	Lower surface capillary force
$f$ , up	Upper surface friction
$f$ , lower	Lower surface friction
leak, 1	Heat leak from evaporator to CC1
leak, 2	Heat leak from evaporator to CC2
TEC, L	Heat absorbed by TEC at the cold side
TEC, H	Heat delivered to the hot side of TEC

#### *Acronyms*

CC	Compensation chamber
DCCLHP	Dual compensation chamber loop heat pipe
ID	Inner diameter
LHP	Loop heat pipe
RTD	Resistance temperature detector
TEC	Thermoelectric Cooler
OD	Outer diameter

## **REFERENCES**

- [1] Y. F. Maydanik. Loop heat pipes. *Applied thermal engineering* 25.5-6 (2005): 635-657.
- [2] A. Ambirajan, A. A. Adoni, J. S. Vaidya, A. A. Rajendran, D. Kumar, P. Dutta. Loop heat pipes: a review of fundamentals, operation, and design. *Heat Transfer Engineering*, 2012, 33(4-5): 387-405.
- [3] B. Siedel, S. Valérie, L. Frédéric. Literature review: Steady-state modelling of loop heat pipes. *Applied Thermal Engineering*, 2015, 75: 709-723
- [4] J. Ku. Operating characteristics of loop heat pipes. *SAE transactions* (1999): 503-519.
- [5] A. Faghri. Review and advances in heat pipe science and technology. *Journal of heat transfer*, 2012, 134(12): 123001-123018.
- [6] M. Mitomi, H. Nagano. Long-distance loop heat pipe for effective utilization of energy. *International Journal of Heat and Mass Transfer*, 2014, 77: 777-784.
- [7] X. Chen, H. Ye, X. Fan, et al. A review of small heat pipes for electronics. *Applied Thermal Engineering*, 2016, 96: 1-17.
- [8] Q. Su, S. Chang, Y. Zhao, et al. A review of loop heat pipes for aircraft anti-icing applications. *Applied Thermal Engineering*, 2018, 130: 528-540.
- [9] Q. Su, S. Chang, M. Song, et al. An experimental study on the heat transfer performance of a loop heat pipe system with ethanol-water mixture as working fluid for aircraft anti-icing. *International Journal of Heat and Mass Transfer*, 2019, 139: 280-292.
- [10] Y. F. Maydanik, S. V. Vershinin, M. A. Chernysheva. Investigation of thermal characteristics of a loop heat pipe in a wide range of external conditions. *International Journal of Heat and Mass Transfer*, 2020, 147: 118967.
- [11] J. Lee, D. Kim, J. Mun, et al. Heat-Transfer Characteristics of a Cryogenic Loop Heat Pipe for Space Applications. *Energies*, 2020, 13(7): 1616.
- [12] G. Lin, H. Zhang, X. Shao, et al. Development and test results of a dual compensation chamber loop heat pipe. *Journal of thermophysics and heat transfer*, 2006, 20(4): 825-834.

- [13] Y. Xie, J. Zhang, L. Xie, et al. Experimental investigation on the operating characteristics of a dual compensation chamber loop heat pipe subjected to acceleration field. *Applied Thermal Engineering*, 2015, 81: 297-312.
- [14] H. Wang, G. Lin, X. Shen, et al. Effect of evaporator tilt on a loop heat pipe with non-condensable gas. *International Journal of Heat and Mass Transfer*, 2019, 128: 1072-1080.
- [15] Y. Xie, Y. Zhou, D. Wen, et al. Experimental investigation on transient characteristics of a dual compensation chamber loop heat pipe subjected to acceleration forces. *Applied Thermal Engineering*, 2018, 130: 169-184.
- [16] D. Gluck, C. Gerhart, S. Stanley. Characterization of a high capacity, dual compensation chamber loop heat pipe. *AIP Conference Proceedings*, 1999, 458(1): 943-948.
- [17] D. Gluck and C. Gerhart. Further investigation of a dual compensation chamber loop heat pipe including hysteresis. *The 11th Annual Spacecraft Thermal Control Technology Workshop*, EI Segundo, CA, 2000.
- [18] C. Gerhart and D. Gluck. "Summary of operating characteristics of a dual compensation chamber loop heat pipe in gravity." *11th International Heat Pipe Conference*, Tokyo, Japan. 1999.
- [19] J. B. Long, J. M. Ochterbeck. Transient/cyclic heat loads for dual compensation chamber loop heat pipes. *proceedings of XI IHPC*, edited by S. Maezawa, Y. Miyazaki, and F. Kaminaga, Japan Association for Heat Pipes, Tokyo, Japan, 1999: 305-310.
- [20] L. Bai, G. Lin, D. Wen, et al. Experimental investigation of start-up behaviors of a dual compensation chamber loop heat pipe with insufficient fluid inventory. *Applied Thermal Engineering*, 2009, 29(8-9): 1447-1456.
- [21] G. Lin, N. Li, L. Bai, et al. Experimental investigation of a dual compensation chamber loop heat pipe. *International Journal of Heat and Mass Transfer*, 2010, 53(15-16): 3231-3240.
- [22] Y. Zhao, S. Chang, B. Yang, et al. Experimental study on the thermal performance of loop heat pipe for the aircraft anti-icing system. *International Journal of Heat and Mass Transfer*, 2017, 111: 795-803.
- [23] L. Bai, Y. Tao, Y. Guo, et al. Start-up characteristics of a dual compensation chamber loop heat pipe with an extended bayonet tube. *International Journal of Heat and Mass Transfer*, 2020, 148: 119066.
- [24] L. Han, Y. Xie, J. Zhu, et al. Experimental and analytical study of dual compensation chamber loop heat pipe under acceleration force assisted condition. *International Journal of Heat and Mass Transfer*, 2020, 153: 119615.
- [25] Y. Xie, X. Li, L. Han, et al. Experimental study on operating characteristics of a dual compensation chamber loop heat pipe in periodic acceleration fields. *Applied Thermal Engineering*, 2020, 176: 115419.
- [26] J. Ku and H. Nagano. Using thermoelectric converters for loop heat pipe operating temperature control. *4th International Energy Conversion Engineering Conference and Exhibit (IECEC)*. 2006: 4057.
- [27] J. Ku and H. Nagano. Loop Heat Pipe Operation with Thermoelectric Converters and Coupling Block. *5th International Energy Conversion Engineering Conference and Exhibit (IECEC)*. 2007: 4713.
- [28] J. Ku and L. Ottenstein. Thermoelectric Converters for Loop Heat Pipe Temperature Control: Experience and Lessons Learned. *40th International Conference on Environmental Systems*. 2010: 6005.
- [29] A. Franzoso, T. Tjptahardja, P. Ruzza, et al. TECLA: a TEC-enhanced Loop Heat Pipe. *43rd International Conference on Environmental Systems*. 2013: 3302.
- [30] R. Yang, G. Lin, J. He, et al. Investigation on the effect of thermoelectric cooler on LHP operation with non-condensable gas. *Applied Thermal Engineering*, 2017, 110: 1189-1199.
- [31] Y. Xie, X. Li, S. Dong, et al. Experimental investigation on operating behaviors of loop heat pipe with thermoelectric cooler under acceleration conditions. *Chinese Journal of Aeronautics*, 2020, 33(3): 852-860.